Article

TMEFF1 is a neuron-specific restriction factor for herpes simplex virus

https://doi.org/10.1038/s41586-024-07670-z

Received: 9 August 2022

Accepted: 4 June 2024

Published online: 24 July 2024

Check for updates

Yao Dai[1,15], Manja Idorn[2,3,15], Manutea C. Serrero[2,3], Xiaoyong Pan[4], Emil A. Thomsen[2,3], Ryo Narita[2,3], Muyesier Maimaitili[2,3], Xiaoqing Qian[5], Marie B. Iversen[2,3], Line S. Reinert[2,3], Rasmus K. Flygaard[6], Muwan Chen[2,3,7], Xiangning Ding[2,3], Bao-cun Zhang[2,3], Madalina E. Carter-Timofte[2,3], Qing Lu[8], Zhuofan Jiang[1], Yiye Zhong[1], Shuhui Zhang[1], Lintai Da[1], Jinwei Zhu[8], Mark Denham[2,7], Poul Nissen[6,7], Trine H. Mogensen[2,3,9], Jacob Giehm Mikkelsen[2,3], Shen-Ying Zhang[10,11], Jean-Laurent Casanova[10,11,12,13], Yujia Cai[1,2,16] ✉ & Søren R. Paludan[2,3,14,16] ✉

The brain is highly sensitive to damage caused by infection and inflammation[1,2]. Herpes simplex virus 1 (HSV-1) is a neurotropic virus and the cause of herpes simplex encephalitis[3]. It is unknown whether neuron-specific antiviral factors control virus replication to prevent infection and excessive inflammatory responses, hence protecting the brain. Here we identify TMEFF1 as an HSV-1 restriction factor using genome-wide CRISPR screening. TMEFF1 is expressed specifically in neurons of the central nervous system and is not regulated by type I interferon, the best-known innate antiviral system controlling virus infections. Depletion of TMEFF1 in stem-cell-derived human neurons led to elevated viral replication and neuronal death following HSV-1 infection. TMEFF1 blocked the HSV-1 replication cycle at the level of viral entry through interactions with nectin-1 and non-muscle myosin heavy chains IIA and IIB, which are core proteins in virus–cell binding and virus–cell fusion, respectively[4–6]. Notably, *Tmeff1*$^{-/-}$ mice exhibited increased susceptibility to HSV-1 infection in the brain but not in the periphery. Within the brain, elevated viral load was observed specifically in neurons. Our study identifies TMEFF1 as a neuron-specific restriction factor essential for prevention of HSV-1 replication in the central nervous system.

Host defence against microbial infections is one of the most fundamental requirements for organisms and species to survive, comparable to having sufficient supplies of food and successful production of offspring. However, immune reactions have the potential to cause severe damage to the host and are highly energy-consuming[7,8]. Therefore, most immune mechanisms are inducible and tightly regulated. Although this is beneficial as a principle to prevent escalation and promote eventual elimination of infection, it does not provide an intrinsic threshold against establishment of infection; nor does it offer full protection of tissues that are highly sensitive to pathogen- or immune-mediated damage. One such tissue is the central nervous system (CNS).

HSV-1 is a highly prevalent neurotropic double-stranded DNA virus with 50–80% of adults being seropositive[3]. Infections are initiated in epithelial cells followed by spread to sensory neurons, most often leading to control of replication and establishment of latency. In rare cases, HSV-1 infection can reach the CNS from the peripheral nerves and cause herpes simplex encephalitis (HSE). This disease has a high mortality rate, and although treatment with acyclovir improves prognosis, there is still a substantial level of mortality with most survivors developing severe neurological sequelae[1]. Defects in the interferon (IFN) arm of the innate immune system predispose to HSE as demonstrated through loss-of-function mutations in several genes of the IFN pathway[9–12]. Recently, disease-causing variants in genes believed to exert cell-intrinsic antiviral activity have also been discovered in patients with HSE[13,14], suggesting that constitutive innate mechanisms are also critically involved in antiviral defence in the brain[8].

Cells in the CNS are isolated from the rest of the body by the blood–brain barrier, hence restricting access of cellular and molecular components. This limits influx of immune cells and inflammatory components into the CNS[15]. At the same time, neurons are highly sensitive to excessive inflammatory responses, and have limited self-renewal capacity[16]. These factors together suggest that neurons have distinct antiviral

[1]Key Laboratory of Systems Biomedicine (Ministry of Education), Shanghai Center for Systems Biomedicine, Shanghai Jiao Tong University, Shanghai, China. [2]Department of Biomedicine, Aarhus University, Aarhus, Denmark. [3]Center for Immunology of Viral Infections, Aarhus, Denmark. [4]Key Laboratory of System Control and Information Processing (Ministry of Education), Institute of Image Processing and Pattern Recognition, Shanghai Jiao Tong University, Shanghai, China. [5]School of Biomedical Engineering, Shanghai Jiao Tong University, Shanghai, China. [6]Department of Molecular Biology and Genetics, Aarhus University, Aarhus, Denmark. [7]Danish Research Institute of Translational Neuroscience, Nordic EMBL Partnership for Molecular Medicine, Aarhus University, Aarhus, Denmark. [8]Key Laboratory for the Genetics of Developmental and Neuropsychiatric Disorders, Ministry of Education, Bio-X Institutes, Shanghai Jiao Tong University, Shanghai, China. [9]Department of Infectious Diseases, Aarhus University Hospital, Aarhus, Denmark. [10]University of Paris, Imagine Institute, Paris, France. [11]St. Giles Laboratory of Human Genetics of Infectious Diseases, The Rockefeller University, New York, NY, USA. [12]Laboratory of Human Genetics of Infectious Diseases, INSERM U1163, Necker Hospital for Sick Children, Paris, France. [13]Howard Hughes Medical Institute, New York, NY, USA. [14]Department of Rheumatology and Inflammation Research, Institute of Medicine, Sahlgrenska Academy, University of Gothenburg, Göteborg, Sweden. [15]These authors contributed equally: Yao Dai, Manja Idorn. [16]These authors jointly supervised this work: Yujia Cai, Søren R. Paludan. ✉e-mail: yujia.cai@sjtu.edu.cn; srp@biomed.au.dk

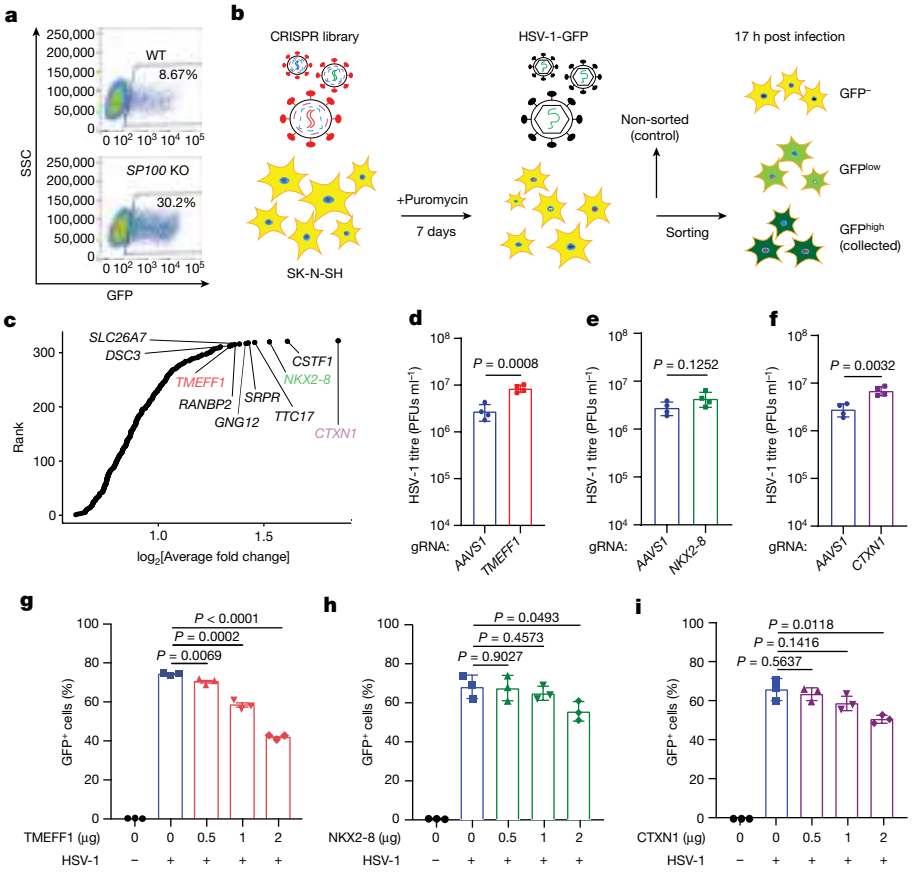

Fig. 1 | Identification of TMEFF1 as an HSV-1 RF expressed in neurons. **a**, SK-N-SH cells were treated with lentivirus encoding Cas9 and gRNA targeting the *SP100* gene, and subsequently infected with HSV-1-GFP (multiplicity of infection (MOI) 0.25). The percentage of GFP$^+$ cells 17 h after infection was evaluated by flow cytometry ($n = 3$). SSC, side scatter. **b**, Schematic illustration of the experimental setup to screen for HSV-1 RFs. **c**, Ranked plot of positively enriched genes supported by a minimum of two individual sgRNAs in both CRISPR screening experiments. Fold-change-based ranking of candidate genes plotted against the average gene level $\log_2$[fold change]. Top-10 ranked genes are labelled; genes mainly expressed in brain tissue are denoted in colour. **d**–**f**, SK-N-SH cells treated with Cas9–guide RNA ribonucleoproteins targeting *TMEFF1*, *NKX2-8*, *CTXN1* or *AAVS1* (as an independent Cas9 target site) were infected with HSV-1 (MOI 0.25). Viral load in culture supernatants 18 h post infection was determined by plaque assay ($n = 4$). PFUs, plaque-forming units. **g**–**i**, HEK293T cells were transfected with increasing amounts of human TMEFF1, NKX2-8 or CTXN1 expression plasmid, and subsequently infected with HSV-1-GFP (MOI 0.5). The percentage of GFP$^+$ cells was analysed 12 h post infection by flow cytometry ($n = 3$). The data are shown as means of biological sample replicates ± s.d. Statistical analysis was carried out using an unpaired two-tailed *t*-test (**d**–**f**) and a two-tailed one-way analysis of variance (ANOVA) test for difference of means, followed by unpaired two-tailed *t*-tests of means indicated by *P* values (**g**–**i**). $P < 0.05$ was considered statistically significant.

strategies, which limit virus replication directly without activating inflammation[17,18]. However, knowledge on the mechanisms governing antiviral defence in neurons remains sparse, and no neuron-specific mechanisms have been identified. In recent years, genome-wide CRISPR screening has emerged as a powerful tool to discover new essential factors in virus–host interactions[19]. For example, CRISPR screens have revealed new receptors of virus, host dependency factors and restriction factors (RFs)[20–24].

To identify neuron-specific HSV-1 RFs, we applied the genome-wide GeCKO v2 CRISPR library in the neuroblastoma cell line SK-N-SH, which exhibits a limited response through the nucleic acid-sensing pathways (Extended Data Fig. 1a–c) and does not evoke an IFN response to HSV-1 infection (Extended Data Fig. 1d,e). In support of using the SK-N-SH cell line, we initially confirmed elevated HSV-1-GFP levels in SK-N-SH cells with knockout of the gene encoding SP100, a known HSV RF[25,26], following infection with HSV-1 expressing GFP from a constitutive CMV promoter (Fig. 1a). Next, SK-N-SH Cas9$^+$ cells were transduced with the lentiviral single guide RNA (sgRNA) library, and then infected with HSV-1-GFP, and the SK-N-SH cells were sorted according to the intensity of GFP fluorescence (Fig. 1b). We carried out two parallel screens to identify candidate RF-encoding genes, by comparing the GFP^{high} population to the unsorted control group. The candidate genes were ranked according to the fold-change enrichment between the unsorted control group and GFP^{high}, allowing identification of a group of 322 genes, each supported in both experiments by at least 2 individual sgRNAs (Extended Data Fig. 1f–i and Supplementary Table 1). The fold-change-based ranking for these genes was plotted against the average fold change. The top-10 ranked genes included *TMEFF1*, *NKX2-8* and *CTXN1*, which are mainly expressed in neuronal tissue (Fig. 1c). Depletion and overexpression of these three genes revealed that *TMEFF1* exhibited the highest potency on the basis of the criteria of being both required and sufficient for restriction of HSV-1 (Fig. 1d–i and Extended Data Fig. 1j). The TMEFF1 protein is a type I transmembrane protein (Extended Data Fig. 2a) expressed primarily in neurons (Extended Data Fig. 2b–d). TMEFF1 is also expressed in the mouse brain, and the overexpression of mouse TMEFF1 in HEK293T cells was sufficient to restrict HSV-1 infection (Extended Data Fig. 2e,f).

Next we generated human neurons from LUHMES embryonic neuronal precursor cells and depleted TMEFF1 and SP100 applying CRISPR–Cas9 technology (Fig. 2a and Extended Data Fig. 3a–c). In TMEFF1-deficient LUHMES neurons, HSV-1 replicated more efficiently with an early increase in the level of gene expression from the viral genome (Fig. 2b and Extended Data Fig. 3d). To examine whether this was also the case in human neurons, we generated cortical neurons

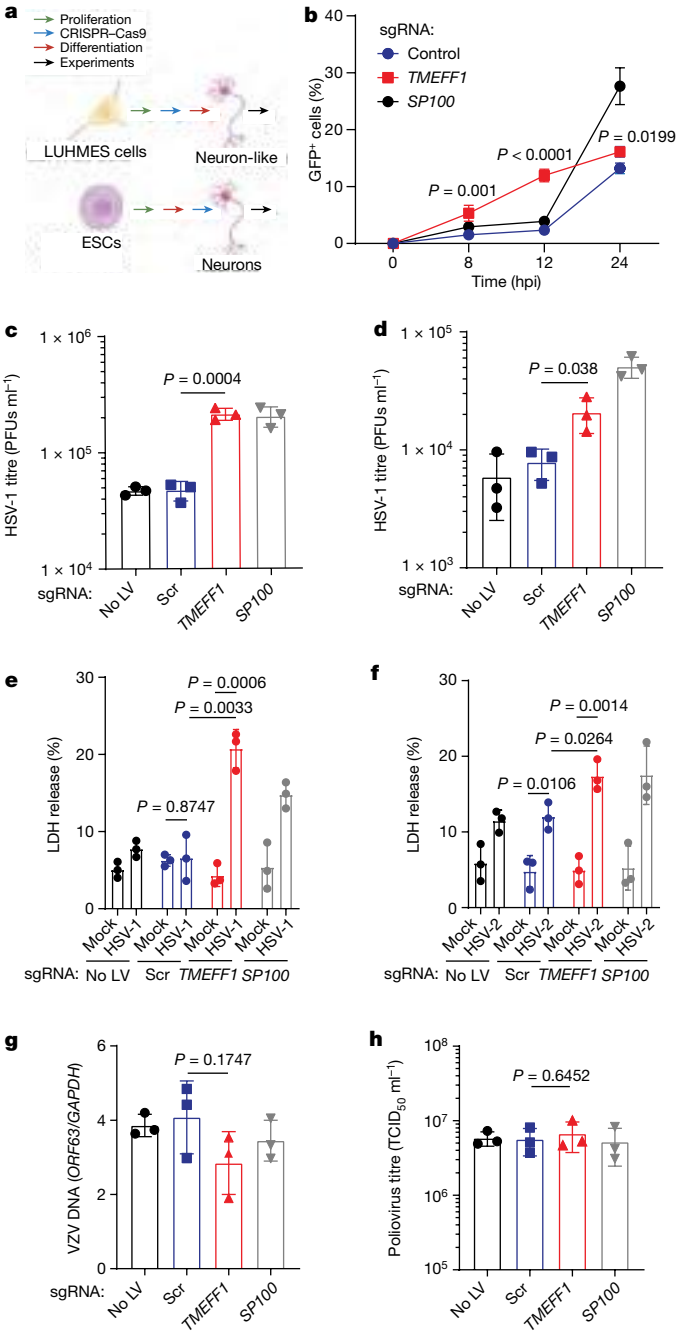

Fig. 2 | TMEFF1 restricts HSV replication in human cortical neurons. **a**, Illustration of the procedures for differentiation of LUHMES cells and ESCs into neurons, including CRISPR–Cas9 genome editing. **b**, LUHMES-derived neurons treated with gRNAs targeting the indicated genes were infected with HSV-1 KOS-64-GFP (MOI 5). Cells were isolated after 8, 12 and 24 h, and examined by flow cytometry for GFP$^+$ signal. Data are presented as percentage of cells that are GFP$^+$ ($n = 3$ biological replicates). hpi, hours post infection. **c**–**f**, hESC-derived cortical neurons were infected with HSV-1 (MOI 1) or HSV-2 (MOI 1). Supernatants were isolated after 24 h of infection for quantification of virus yield (**c**,**d**), and after 72 h of infection for measurement of lactate dehydrogenase activity (LDH; **e**,**f**; $n = 3$). LV, lentivirus; Scr, scrambled guide RNA. **g**,**h**, hESC-derived cortical neurons were infected with VZV (cell-free, 350 viral genomes per cell) or poliovirus (MOI 0.1). Total DNA was isolated from VZV-infected cells 24 h after infection, and supernatants were isolated from the poliovirus-infected cultures 16 h after infection for evaluation of VZV DNA by quantitative PCR and viral load by 50% tissue culture infectious dose ($TCID_{50}$) assay, respectively ($n = 3$ biological replicates). The data are shown as means of biological sample triplicates ± s.d. Statistical analysis was carried out using a two-tailed one-way ANOVA (**c**,**d**,**g**,**h**) and a two-tailed two-way ANOVA (**b**,**e**,**f**) test for difference of means, followed by unpaired two-tailed *t*-tests of means of Scr (or control) and TMEFF1 groups indicated by *P* values. $P < 0.05$ was considered statistically significant. Illustration in **a** was created using BioRender.com.

from human embryonic stem cells (hESCs), and knocked out *TMEFF1* (Fig. 2a and Extended Data Fig. 3e–h). The cells were infected with a panel of neurotropic viruses. Disruption of *TMEFF1* led to an elevated level of replication of HSV-1, and to a lesser extent also of HSV-2, both belonging to the *simplex* genera of alphaherpesviruses (Fig. 2c,d). The elevated level of viral replication in the TMEFF1-depleted cells was accompanied by a significant level of neuronal cell death (Fig. 2e,f). By contrast, replication of two other neurotropic viruses, varicella zoster virus (VZV; *varicello* genus of alphaherpesviruses) and poliovirus (picornavirus), was not affected by depletion of TMEFF1 (Fig. 2g,h).

To gain insight into the role of TMEFF1 in control of HSV-1 in vivo, we utilized *Tmeff1*$^{-/-}$ mice generated by gene trapping (Extended Data Fig. 4a–e). Ocular HSV-1 infection in mice leads to spread to the CNS through the neuronal route and development of encephalitis-like disease[27], thus sharing some resemblance with HSE (in children) after primary infection. *Tmeff1*$^{-/-}$ mice exhibited lower survival rates following HSV-1 infection compared to wild-type (WT) littermate controls, comparable to that of *Irf3*$^{-/-}$ mice, but not as profound as that of *Ifnar1*$^{-/-}$ mice (Fig. 3a). Likewise, HSV-1-infected *Tmeff1*$^{-/-}$ mice developed accelerated weight loss and elevated disease symptom scores, again comparable to those of *Irf3*$^{-/-}$ mice (Extended Data Fig. 4f,g). Following ocular infection, HSV-1 infects the cornea and is transported through trigeminal ganglia to the brain region[27]. Mouse *Tmeff1* was expressed in the brainstem, but not in eyes or trigeminal ganglia (Fig. 3b), and consistently, we observed elevated viral titres in the brainstem, but not in the trigeminal ganglia or in eye washes, from *Tmeff1*$^{-/-}$ mice compared to WT littermates (Fig. 3c–e). Immunohistochemical staining for HSV-1 antigen in brainstem sections showed an increased number of HSV-1$^+$ cells in the TMEFF1-deficient mice (Fig. 3f,g). *Tmeff1* is expressed at much higher levels in neurons than in microglia and astrocytes (Extended Data Fig. 5a), and in vitro infection of WT and *Tmeff1*$^{-/-}$ neurons, astrocytes and microglia led to an elevated level of viral replication in *Tmeff1*$^{-/-}$ neurons but not astrocytes or microglia compared to the corresponding WT cells (Fig. 3h and Extended Data Fig. 5d). In support of the neuron-specific action of TMEFF1 also in vivo, immunohistochemical staining of brainstem sections for HSV-1 and cell type markers revealed that TMEFF1 deficiency led to an increase in the percentage of HSV-1$^+$ neurons (Fig. 3i,j), but not HSV-1$^+$ astrocytes (Fig. 3k and Extended Data Fig. 5b,c). Although the above data were from *Tmeff1*$^{-/-}$ mice and WT littermate controls on a mixed background, we also backcrossed the mice for ten generations onto a C57BL/6N background. HSV-1 challenge experiments corroborated that the *Tmeff1*$^{-/-}$ mice on a pure C57BL/6N background retained the increased susceptibility to HSV-1 infection and significantly decreased survival rates compared to the WT (Extended Data Fig. 5e–g). These data demonstrate that TMEFF1 is essential for HSV-1 restriction in an in vivo model of HSE.

To explore the mechanism of action of TMEFF1, we first tested whether TMEFF1 expression is regulated by IFNs or inflammatory cytokines. Examination of hESC-derived neurons and SK-N-SH cells showed that TMEFF1 was constitutively expressed at high levels and not altered by cytokine stimulation (Extended Data Fig. 6a–f). Likewise, TMEFF1 expression did not affect the activity of type I IFN (Extended Data Fig. 6g). This suggests that TMEFF1 acts through a constitutive mechanism independent of the type I IFN system. To map the step in the viral replication cycle targeted by TMEFF1, we expressed TMEFF1 in HEK293T cells. Incubation with WT HSV-1 and entry-deficient mutants (Δ*gD*, impaired cell binding; Δ*gB*, defective virus–cell fusion)

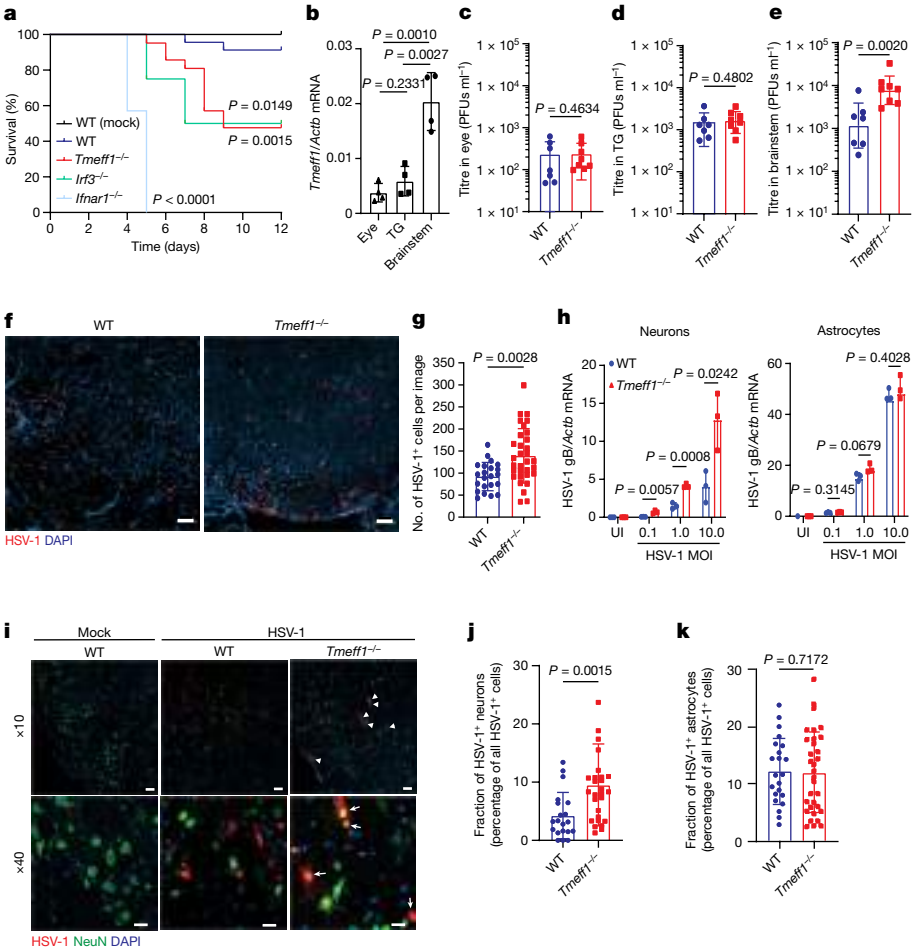

Fig. 3 | TMEFF1 is essential for host defence against HSV-1 brain infection in mice. a, WT, *Irf3*$^{-/-}$, *Ifnar1*$^{-/-}$ and *Tmeff1*$^{-/-}$ mice were infected with HSV-1 (cornea, 2×10^6 PFUs per eye) and monitored for survival (mock WT, $n = 5$; infected WT, $n = 12$; *Tmeff1*$^{-/-}$, $n = 7$; *Irf3*$^{-/-}$, $n = 5$; *Ifnar1*$^{-/-}$, $n = 7$). **b**, *Tmeff1* mRNA levels (C57BL/6) in eyes, trigeminal ganglia (TG) and brainstems ($n = 4$). **c**–**e**, Viral load in eye washes (day 2 post infection; **c**), trigeminal ganglia (day 5 post infection; **d**) and brainstem (day 5 post infection; **e**). (WT, $n = 7$; *Tmeff1*$^{-/-}$, $n = 8$.) **f**, HSV-1 gB and 4′,6-diamidino-2-phenylindole (DAPI) staining of tissue slices of the brainstem (day 5 post infection). Scale bars, 50 µm. **g**, Quantification of staining in **f** (WT, $n = 22$; *Tmeff1*$^{-/-}$, $n = 31$). **h**, HSV-1 *gB* mRNA after 24 h HSV-1 infection of primary mouse astrocyte (right) and neuron (left) cultures ($n = 3$ biological replicates and 3 independent experiments). UI, uninfected. **i**, Brainstem slices from HSV-1-infected WT and *Tmeff1*$^{-/-}$ littermates (day 5 post infection) stained for HSV-1 and NeuN (neurons) and visualized by fluorescence microscopy. Arrows indicate cells that are double-positive for HSV-1 and NeuN. Scale bars, 50 µm (top row) and 20 µm (bottom row). **j**,**k**, Quantification of co-localization of HSV-1–NeuN (WT, $n = 20$; *Tmeff1*$^{-/-}$, $n = 31$; **j**; quantification of **i**) and HSV-1–S100 (WT, $n = 22$; *Tmeff1*$^{-/-}$, $n = 32$; **k**; Extended Data Fig. 5c). Brainstems imaged: WT, $n = 4$; *Tmeff1*$^{-/-}$, $n = 5$. Each brainstem is represented by images of three different anatomic bregma. Only images containing HSV-1 foci were quantified. Statistical analysis: **a**, log-rank Mantel–Cox test; **b**,**h**, two-tailed one-way ANOVA test for difference of means, followed by unpaired two-tailed *t*-tests of means of groups indicated by *P* values; **c**–**e**,**g**,**j**,**k**, non-parametric two-tailed Mann–Whitney *U*-tests. Error bars, ±s.d. *P* values < 0.05 were considered statistically significant.

at 4 °C, at which virus entry does not occur, showed that TMEFF1 did not block viral attachment to cells (Extended Data Fig. 6h,i). By contrast, TMEFF1-overexpression led to decreased HSV-1 DNA levels in both cytoplasm plus membrane and nuclear fractions (Extended Data Fig. 6j), and a reduced level of accumulation of the viral capsid protein VP5 in cytoplasmic lysates (Extended Data Fig. 6k). Transmission electron microscopy revealed that accumulation of viral capsids in the nuclear periphery of HEK293T cells accompanied by chromatin condensation and margination 12 h post HSV-1 infection was absent in TMEFF1-overexpressing cells as opposed to the case in unmodified cells (Extended Data Fig. 6l,m). Corroborating these data, lower virus yield was obtained from TMEFF1-expressing cells following HSV-1 infection, but not when the viral genome was delivered in a manner bypassing the natural entry-route through transfection of viral DNA (Extended Data Fig. 6n). Next we tracked HSV-1 at different time points post infection, using fluorescence microscopy and an HSV-1 mutant containing GFP protein fused to the viral capsid protein VP26 (HSV-1 K26GFP)[28]. Whereas the virus localized to the plasma membrane at time zero irrespective of TMEFF1 expression, the virus localization shifted inwards over time to the cytoplasm and the nucleus in the control cells, but not in the TMEFF1-expressing cells (Fig. 4a). In agreement with these data, our results show that *TMEFF1* knockout in hESC- and LUHMES-derived neurons reduced the level of HSV-1 entry as measured by early localization of viral capsids at the nuclear rim (Fig. 4b and Extended Data Fig. 6o). Most proteins involved in HSV-1 entry, such as gD or gB receptors, were expressed in the cell lines and neurons used in this study (Extended Data Fig. 6p). Taken together, these findings demonstrate that TMEFF1 exerts antiviral activity by preventing HSV-1 cellular entry.

We next searched for proteins interacting with HA-tagged TMEFF1 using co-immunoprecipitation. A unique >170-kDa band was isolated, and mass spectrometric analysis led to identification of 29 peptides from non-muscle myosin heavy chain (NMHC)-IIA and 11 peptides from NMHC-IIB (Extended Data Fig. 7a,b). Split GFP[29] and co-immunoprecipitation confirmed the association between TMEFF1

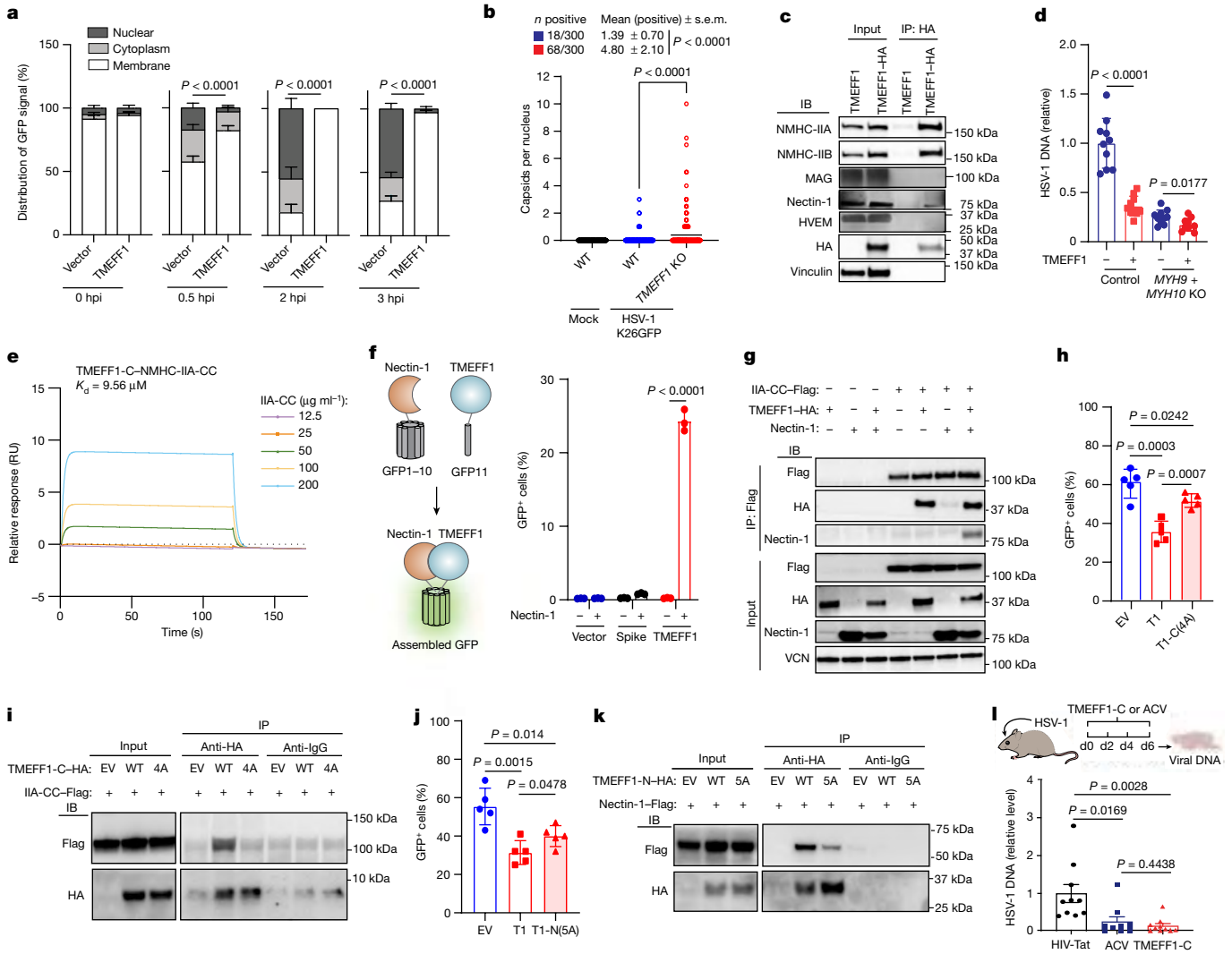

Fig. 4 | TMEFF1 prevents HSV-1 entry through interactions with nectin-1, NMHC-IIA and NMHC-IIB. a, Subcellular localization of HSV-1 in HEK293T cells infected with HSV-1 K26GFP (MOI 100; 102, 114, 104 and 107 cells counted per group). **b**, GFP$^+$ spots in hESC-derived WT and TMEFF1-deficient neurons infected with HSV-1 K26GFP (MOI 50) for 2 h. GFP$^+$ spots were quantified blinded (300 cells per group). **c**, Anti-HA-immunoprecipitated lysates from hESC-derived neurons transduced as shown were immunoblotted for NMHC-IIA, NMHC-IIB, MAG, nectin-1, HVEM, HA and vinculin. IP, immunoprecipitation; IB, immunoblot. **d**, Nuclear HSV-1 DNA in HEK293T cells null for *MYH9* and *MYH10* and transfected with TMEFF1. HSV-1, MOI 0.5, 3 h (n = 10 biological replicates per group). KO, knockout. **e**, GST–TMEFF1-C peptide was immobilized and IIA-CC was analysed by plasmon surface resonance. RU, response units. **f**, HEK293T cells transfected with GFP1–10–nectin-1 and GFP11–TMEFF1 or SARS-CoV-2 spike (graphically illustrated to the left) were analysed by flow cytometry (right) (n = 3 biological replicates). **g**, Anti-Flag-immunoprecipitated lysates from HEK293T cells transfected as shown were immunoblotted with the indicated antibodies. **h**,**j**, HEK293T cells transfected with WT TMEFF1 (T1), TMEFF1-C(Q366A/L368A,H370A/F371A) (T1-C(4A)) or TMEFF1-N(R126A/K130A/F199A/Y292A/Q295A) (T1-N(5A)) as indicated were infected with HSV-1-GFP (MOI 0.5), and analysed by flow cytometry (n = 5 biological replicates). EV, empty vector. **i**,**k**, Anti-HA-immunoprecipitated lysates from HEK293T cells transfected as described in **h**,**j** were immunoblotted with anti-Flag and anti-HA. **l**, Mice treated with TMEFF1-C or HIV-Tat peptide (8 μl, 80 μM) or acyclovir (ACV, 8 μl, 40 μM) were infected with HSV-1 (cornea, 2.6 × 10^6 PFUs per eye), and brainstems were isolated day 6 (d6) post infection for measurement of HSV-1 DNA (n = 10). All data are representative of at least three independent experiments. Statistics: two-tailed two-way ANOVA test (**a**,**d**,**f**) or a two-tailed one-way ANOVA (**b**,**h**,**j**,**l**) test, followed by unpaired two-tailed t-tests of means of groups indicated by P values (**a**–**c**,**f**,**j**,**l**,**n**,**o**). Error bars, ±s.d. P < 0.05 was considered statistically significant. For gel source data, see Supplementary Fig. 1. Illustrations of treatment schedule and viral DNA in **l** were created with BioRender.com.

and both NMHC-IIA and NMHC-IIB (Extended Data Fig. 7c–g). In this system, nectin-1 also co-immunoprecipitated with TMEFF1 (Extended Data Fig. 7d). Notably, the endogenous NMHC-IIA, NMHC-IIB and nectin-1 proteins, but not the two HSV-1-entry-related proteins HVEM and MAG[30,31], were co-immunoprecipitated with TMEFF1–HA introduced by lentiviral transduction in hESC-derived neurons (Fig. 4c). Nectin-1 is an HSV-1 gD receptor[4], and NMHC-IIA and NMHC-IIB have been reported to be involved in HSV-1 entry through gB[5,6], with NMHC-IIB recently being shown to act downstream of nectin-1 in HSV-1 entry in neurons[32]. Accordingly, HSV-1 progeny yield was significantly reduced in cells null for *MYH9* and *MYH10* (encoding NMHC-IIA and NMHC-IIB) and *NECTIN1* (Extended Data Fig. 7h–m), hence linking NMHC-IIA and NMHC-IIB to nectin-1-dependent HSV-1 entry in the cell systems used in this study. TMEFF1, nectin-1, NMHC-IIA and NMHC-IIB are highly conserved between human and mice (Extended Data Fig. 7n). Expression of TMEFF1 in HEK293T cells null for *MYH9* and *MYH10* reduced, but did not abrogate, its antiviral activity (Fig. 4d and Extended Data Fig. 7o). Additionally, TMEFF1 impaired HSV-1 replication after entry mediated by either nectin-1 or HVEM, with a stronger effect on nectin-1-dependent entry (Extended Data Fig. 7p,q). These data suggest important roles

for nectin-1, NMHC-IIA and NMHC-IIB in TMEFF1-mediated blockage of HSV-1 entry.

To identify the regions of TMEFF1 engaged in protein–protein interactions with NMHC-II and nectin-1, we expressed two truncated versions of TMEFF1, namely the extracellular amino-terminal region and the carboxy-terminal cytoplasmic domain. For NMHC-IIA, we expressed the motor and the coiled coil (CC) domains, and for nectin-1, we expressed the extracellular and cytoplasmic regions (Extended Data Fig. 8a). In HEK293T cells, TMEFF1 co-immunoprecipitated with the NMHC-IIA CC domain (Extended Data Fig. 8b), which in turn could be precipitated with the C-terminal domain of TMEFF1 (Extended Data Fig. 8c). Likewise, the N-terminal portion of TMEFF1 co-immunoprecipitated with nectin-1 (Extended Data Fig. 8d). Surface plasmon resonance and glutathione *S*-transferase (GST) pull-down confirmed the interaction between the cytoplasmic domain of TMEFF1 and the NMHC-IIA CC domain (Fig. 4e and Extended Data Fig. 8e). The interaction between TMEFF1 and nectin-1 was confirmed by split GFP (Fig. 4f). Finally, we tested whether TMEFF1, NMHC-IIA, NMHC-IIB and nectin-1 may be engaged in a ternary complex through co-immunoprecipitations in HEK293T cells. Indeed, nectin-1 was co-immunoprecipitated with NMHC-IIA-CC only in cells expressing TMEFF1 (Fig. 4g).

To test whether TMEFF1 exerts its anti-HSV-1 activity through the identified protein–protein interactions, we used AlphaFold to predict possible interaction surfaces. The predicted models suggested putative interactions between the two pairs of proteins, and two models were selected to be most likely (Extended Data Fig. 9a,b). We carried out en bloc alanine substitutions of the five residues in the N-terminal domain of TMEFF1 predicted to constitute the interaction surfaces with nectin-1, and also of the four residues in the C-terminal domain of TMEFF1 predicted to constitute the interaction surface with NMHC-IIA and NMHC-IIB. Notably, both sets of substitutions reduced the antiviral activity of TMEFF1, as well as the level of co-immunoprecipitation between TMEFF1-C and NMHC-IIA-CC and between TMEFF-N and nectin-1-N (Fig. 4h–k). To further explore the contribution from the cytoplasmic domain of TMEFF1 to the antiviral activity, we generated a cell-permeable peptide through fusion with HIV1 TAT peptide (Extended Data Fig. 9c). The TMEFF1-C peptide exhibited anti-HSV-1 activity in HEK293T cells in a NMHC-IIA- and NMHC-IIB-dependent manner (Extended Data Fig. 9d–h), and blocked HSV-1 entry into LUHMES-derived neurons (Extended Data Fig. 9i). Finally, the TMEFF1-C peptide showed potent antiviral activity in vivo (Fig. 4l and Extended Data Fig. 9j,k). These data collectively suggest that TMEFF1 associates with nectin-1, NMHC-IIA and NMHC-IIB in the HSV-1 entry machinery to block viral entry.

We report TMEFF1 as a neuron-specific RF, which plays a non-redundant role in restriction of HSV-1 in CNS neurons (Extended Data Fig. 10). TMEFF1 is a transmembrane protein located in the plasma membrane, and forms a family together with TMEFF2 (ref. 33). It has previously been demonstrated that recombinant TMEFF2 protein can promote survival of neurons in vitro[33], but the function of TMEFF1 in neurons is not well characterized[34]. We found that TMEFF1 blocks HSV-1 entry, and interacts with nectin-1, NMHC-IIA and NMHC-IIB[5,6,32]. Although we were initially testing a hypothesis of restriction through a single mechanism, our data indicate that the interactions with nectin-1, NMHC-IIA and NMHC-IIB contribute to the full antiviral activity. This suggests that TMEFF1 restricts both nectin-1- and HVEM-mediated entry, with the former being controlled most efficiently. Hence, TMEFF1 targets both gD-dependent and gB-dependent steps in HSV-1 entry. There are several examples in the literature of RFs using more than one mechanism to restrict viral replication[35–40].

TMEFF1 is expressed constitutively in human and mouse CNS neurons, and the expression is not regulated by IFNs and inflammatory cytokines. Experiments in *Tmeff1*$^{-/-}$ mice and hESC-derived neurons revealed an important role for TMEFF1 in control of HSV-1 replication and prevention of brain infection. Although a number of HSV-1 RFs have been reported, including MxB[41], IFI16 (ref. 42) and PML nuclear body proteins[26], most of these act at the level of nuclear DNA delivery, viral transcription or viral DNA replication. Most known HSV-1 RFs are IFN-regulated[43], and none has been reported to be expressed predominantly in neurons. To our knowledge, the present finding represents the first report of a neuron-specific HSV-1 RF, acting independently of the IFN system. The finding that TMEFF1 uses a dual mechanism to restrict HSV-1 may underscore the physiological importance of excluding this virus, which is highly abundant in the human population, from the CNS.

Immune responses to infection are fine balances between elimination of the pathogen and immune-mediated tissue damage. This is particularly challenging in the brain, in which both innate and adaptive immune responses can cause devastating pathology. For instance, although the type I IFN system is central for control of HSV-1 replication in the brain[9–12], excessive IFN activity leads to pathology as illustrated in Aicardi–Goutières syndrome[2]. Recent studies have revealed genetic defects in type I IFN-independent antiviral mechanisms in patients with DNA virus infection acting to control viral replication and prevent disease in the CNS[13,14,18,44]. Collectively, the available data suggest that optimal antiviral immune responses in the brain represent a combination of constitutive and IFN-driven immune mechanisms[16]. Whereas the former exerts immediate restriction and elevates the threshold for establishment of infection, the latter is more powerful, but also has the potential to cause tissue damage. In conclusion, through the identification of TMEFF1 as a RF, we uncover a new neuron-specific immunological mechanism that protects cortical neurons against viral infection.

Online content

Any methods, additional references, Nature Portfolio reporting summaries, source data, extended data, supplementary information, acknowledgements, peer review information; details of author contributions and competing interests; and statements of data and code availability are available at https://doi.org/10.1038/s41586-024-07670-z.

1. Stahl, J. P. & Mailles, A. Herpes simplex virus encephalitis update. *Curr. Opin. Infect. Dis.* **32**, 239–243 (2019).
2. Crow, Y. J. & Manel, N. Aicardi–Goutières syndrome and the type I interferonopathies. *Nat. Rev. Immunol.* **15**, 429–440 (2015).
3. Liesegang, T. J. Herpes simplex virus epidemiology and ocular importance. *Cornea* **20**, 1–13 (2001).
4. Geraghty, R. J., Krummenacher, C., Cohen, G. H., Eisenberg, R. J. & Spear, P. G. Entry of alphaherpesviruses mediated by poliovirus receptor-related protein 1 and poliovirus receptor. *Science* **280**, 1618–1620 (1998).
5. Arii, J. et al. Non-muscle myosin IIA is a functional entry receptor for herpes simplex virus-1. *Nature* **467**, 859–862 (2010).
6. Arii, J., Hirohata, Y., Kato, A. & Kawaguchi, Y. Nonmuscle myosin heavy chain IIb mediates herpes simplex virus 1 entry. *J. Virol.* **89**, 1879–1888 (2015).
7. Casanova, J. L. Human genetic basis of interindividual variability in the course of infection. *Proc. Natl Acad. Sci. USA* **112**, E7118–E7127 (2015).
8. Paludan, S. R., Pradeu, T., Master, S. & Mogensen, T. H. Constitutive immune mechanisms: mediators of host defence and immune regulation. *Nat. Rev. Immunol.* **21**, 137–150 (2021).
9. Zhang, S. Y. et al. TLR3 deficiency in patients with herpes simplex encephalitis. *Science* **317**, 1522–1527 (2007).
10. Herman, M. et al. Heterozygous TBK1 mutations impair TLR3 immunity and underlie herpes simplex encephalitis of childhood. *J. Exp. Med.* **209**, 1567–1582 (2012).
11. Andersen, L. L. et al. Functional IRF3 deficiency in a patient with herpes simplex encephalitis. *J. Exp. Med.* **212**, 1371–1379 (2015).
12. Bastard, P. et al. Herpes simplex encephalitis in a patient with a distinctive form of inherited IFNAR1 deficiency. *J. Clin. Investig.* https://doi.org/10.1172/JCI139980 (2021).
13. Zhang, S. Y. et al. Inborn errors of RNA lariat metabolism in humans with brainstem viral infection. *Cell* **172**, 952–965 (2018).
14. Lafaille, F. G. et al. Human SNORA31 variations impair cortical neuron-intrinsic immunity to HSV-1 and underlie herpes simplex encephalitis. *Nat. Med.* **25**, 1873–1884 (2019).
15. Chakraborty, S., Nazmi, A., Dutta, K. & Basu, A. Neurons under viral attack: victims or warriors? *Neurochem. Int.* **56**, 727–735 (2010).
16. Paludan, S. R. & Mogensen, T. H. Constitutive and latent immune mechanisms exert 'silent' control of virus infections in the central nervous system. *Curr. Opin. Immunol.* **72**, 158–166 (2021).
17. Yordy, B., Iijima, N., Huttner, A., Leib, D. & Iwasaki, A. A neuron-specific role for autophagy in antiviral defense against herpes simplex virus. *Cell Host. Microbe* **12**, 334–345 (2012).

18. Hait, A. S. et al. Defects in LC3B2 and ATG4A underlie HSV2 meningitis and reveal a critical role for autophagy in antiviral defense in humans. *Sci. Immunol.* **5**, eabc2691 (2020).
19. Shalem, O. et al. Genome-scale CRISPR-Cas9 knockout screening in human cells. *Science* **343**, 84–87 (2014).
20. Pillay, S. et al. An essential receptor for adeno-associated virus infection. *Nature* **530**, 108–112 (2016).
21. Zhang, R. et al. Mxra8 is a receptor for multiple arthritogenic alphaviruses. *Nature* **557**, 570–574 (2018).
22. Park, R. J. et al. A genome-wide CRISPR screen identifies a restricted set of HIV host dependency factors. *Nat. Genet.* **49**, 193–203 (2017).
23. Baggen, J. et al. Genome-wide CRISPR screening identifies TMEM106B as a proviral host factor for SARS-CoV-2. *Nat. Genet.* **53**, 435–444 (2021).
24. Wei, J. et al. Genome-wide CRISPR screens reveal host factors critical for SARS-CoV-2 infection. *Cell* **184**, 76–91 (2021).
25. Negorev, D. G., Vladimirova, O. V., Ivanov, A., Rauscher, F. 3rd & Maul, G. G. Differential role of Sp100 isoforms in interferon-mediated repression of herpes simplex virus type 1 immediate-early protein expression. *J. Virol.* **80**, 8019–8029 (2006).
26. Xu, P. & Roizman, B. The SP100 component of ND10 enhances accumulation of PML and suppresses replication and the assembly of HSV replication compartments. *Proc. Natl Acad. Sci. USA* **114**, E3823–E3829 (2017).
27. Reinert, L. S. et al. Sensing of HSV-1 by the cGAS-STING pathway in microglia orchestrates antiviral defense in the CNS. *Nat. Commun.* **7**, 13348 (2016).
28. Desai, P. & Person, S. Incorporation of the green fluorescent protein into the herpes simplex virus type 1 capsid. *J. Virol.* **72**, 7563–7568 (1998).
29. Cabantous, S., Terwilliger, T. C. & Waldo, G. S. Protein tagging and detection with engineered self-assembling fragments of green fluorescent protein. *Nat. Biotechnol.* **23**, 102–107 (2005).
30. Montgomery, R. I., Warner, M. S., Lum, B. J. & Spear, P. G. Herpes simplex virus-1 entry into cells mediated by a novel member of the TNF/NGF receptor family. *Cell* **87**, 427–436 (1996).
31. Suenaga, T. et al. Myelin-associated glycoprotein mediates membrane fusion and entry of neurotropic herpesviruses. *Proc. Natl Acad. Sci. USA* **107**, 866–871 (2010).
32. Wang, C. et al. Nectin-1 and non-muscle myosin heavy chain-IIB: major mediators of herpes simplex virus-1 entry into corneal nerves. *Front. Microbiol.* **13**, 830699 (2022).
33. Horie, M. et al. Identification and characterization of TMEFF2, a novel survival factor for hippocampal and mesencephalic neurons. *Genomics* **67**, 146–152 (2000).
34. Kanemoto, N. et al. Expression of TMEFF1 mRNA in the mouse central nervous system: precise examination and comparative studies of TMEFF1 and TMEFF2. *Mol. Brain Res.* **86**, 48–55 (2001).
35. Laguette, N. et al. SAMHD1 is the dendritic- and myeloid-cell-specific HIV-1 restriction factor counteracted by Vpx. *Nature* **474**, 654–657 (2011).
36. Ryoo, J. et al. The ribonuclease activity of SAMHD1 is required for HIV-1 restriction. *Nat. Med.* **20**, 936–941 (2014).
37. Li, K. et al. IFITM proteins restrict viral membrane hemifusion. *PLoS Pathog.* **9**, e1003124 (2013).
38. Lanz, C. et al. IFITM3 incorporation sensitizes influenza A virus to antibody-mediated neutralization. *J. Exp. Med.* https://doi.org/10.1084/jem.20200303 (2021).
39. Xu, D. et al. PLSCR1 is a cell-autonomous defence factor against SARS-CoV-2 infection. *Nature* **619**, 819–827 (2023).
40. Kusano, S. & Ikeda, M. Interaction of phospholipid scramblase 1 with the Epstein-Barr virus protein BZLF1 represses BZLF1-mediated lytic gene transcription. *J. Biol. Chem.* **294**, 15104–15116 (2019).
41. Crameri, M. et al. MxB is an interferon-induced restriction factor of human herpesviruses. *Nat. Commun.* **9**, 1980 (2018).
42. Orzalli, M. H., Conwell, S. E., Berrios, C., DeCaprio, J. A. & Knipe, D. M. Nuclear interferon-inducible protein 16 promotes silencing of herpesviral and transfected DNA. *Proc. Natl Acad. Sci. USA* **110**, E4492–E4501 (2013).
43. Alandijany, T. Host intrinsic and innate intracellular immunity during herpes simplex virus type 1 (HSV-1) infection. *Front. Microbiol.* **10**, 2611 (2019).
44. Brinck Andersen, N. S. et al. Essential role of autophagy in restricting poliovirus infection revealed by identification of an ATG7 defect in a poliomyelitis patient. *Autophagy* https://doi.org/10.1080/15548627.2020.1831800 (2020).

Methods

Cell lines and viruses

HEK293T, HeLa, SK-N-SH and SH-SY5Y (derived from SK-N-SH) cells were cultured in DMEM (Sigma Aldrich) and RPMI-1640 (Sigma Aldrich) with L-glutamine supplemented with 10% heat-inactivated FBS (Life Technologies), 1% penicillin–streptomycin (Life Technologies). All cell lines were tested and negative for mycoplasma. For experiments, cells were seeded in tissue culture plates at a density of about $0.2–2.0 \times 10^5$ cells per square centimetre and incubated overnight at 37 °C and 5% CO_2 before use. The viruses used for experiments were HSV-1 (strains KOS and McKrae), HSV-1 KOS-64-GFP[45], HSV-1 K26GFP[28], HSV-1 Δ*gB*[46], HSV-1 Δ*gD*[47], HSV-2 (333 strain), poliovirus 1 (LSa strain) and VZV (ROka strain). HSV-1 genomic viral DNA was isolated from purified nucleocapsids as described previously[48]. HSV-1 and HSV-2 were grown and titrated on Vero cells, poliovirus was grown and titrated on HeLa cells, and VZV was propagated in MeWo cells.

Antibodies

The following antibodies were used: rabbit anti-MYH9 (NMHC-IIA) (Proteintech, number 11128-1-AP), rabbit anti-MYH10 (NMHC-IIB) (Proteintech, number 19673-1-AP), mouse anti-TMEFF1 (Santa Cruz, number sc-393457), goat anti-mouse TMEFF1 (R&D Systems, number AF1995-SP), rabbit anti-Flag (Proteintech, number 20543-1-AP), mouse anti-HA (Proteintech, number 66006-1-Ig), mouse anti-HA (Proteintech, number 60008-1-Ig), mouse anti-GST (Abmart, number M20007); mouse monoclonal anti-VP5 (Abcam, number ab6508), rabbit polyclonal anti-HSV (Dako; number GA521), mouse monoclonal anti-NeuN (Merck Millipore, clone A60), mouse monoclonal anti-S100 (Abcam, clone 4C4.9), chicken anti-MAP2 (Abcam, number ab92434), mouse monoclonal anti-TUBB3 (Millipore, number MAB1637).

Genome-wide CRISPR screen

For the genome-wide CRISPR screen, we used the GeCKO v2 CRISPR library and $Cas9^+$ SK-N-SH cells. Raw sequencing reads were processed to remove known adaptor sequences located 5′ and 3′ of the 20-base-pair sgRNA sequence using cutadapt 3.7. Using MAGeCK v0.5.9.4, trimmed reads were mapped to unique sgRNAs resulting in quantified read counts of individual sgRNAs, summarized read counts and screen descriptive data available in Supplementary Table 1. Using MAGeCK, each experiment was analysed by comparing the GFP^{high} sample to the unsorted control. On the basis of gene fold change, we ranked the enriched genes and focused on genes identified by at least two individual sgRNAs in both experiments.

Culture, differentiation and manipulation of LUHMES cells

LUHMES cells were seeded onto dishes coated with poly-L-ornithine (Sigma Aldrich) and fibronectin (Sigma Aldrich). Undifferentiated LUHMES cells were maintained in proliferation medium DMEM/F-12 (Gibco) supplemented with 1% N-2 (Gibco) and 40 ng ml^{-1} β-FGF (R&D Systems). LUHMES-derived neurons were obtained after 7 days of incubation in differentiation medium DMEM/F-12 supplemented with 1% N-2, 10 μg ml^{-1} tetracycline (Sigma Aldrich), 1 mM dibutyryl cAMP (Sigma Aldrich) and 20 ng ml^{-1} GDNF (R&D Systems). In all cases, medium was renewed every 2 days.

hESC-derived cortical neurons

Human neurons were generated as previously described[49]. Briefly, hESCs (WA-09, WiCell) were maintained on Vitronectin-coated (STEMCELL Technologies) 35-mm-diameter Petri dishes (Thermo Scientific) in TeSR-E8 basal medium (STEMCELL Technologies). Two days before the direct conversion, 2.5×10^4 cells were plated on a Vitronectin-coated 35-mm-diameter Petri dish in TeSR-E8 basal medium with 10 μM Y-27632. On day −1, cells were transduced with the lentiviral plasmids FUW-M2rtTA and Tet-O-Ngn2-puro (Addgene plasmid numbers 20342 and 52047) with a total MOI of 50 in E8 medium. On day 0, cells were washed with PBS++ once, and culture medium was replaced with N2B27 medium containing 1:1 of Neurobasal medium and DMEM/F-12 supplemented with N-2 supplement 1%, B-27 supplement minus vitamin A 1%, insulin–transferrin–selenium-A 1%, glucose 0.3%, GlutaMAX supplement 0.5%, penicillin–streptomycin 0.5% (all from Life Technologies) and doxycycline (1 μg ml^{-1}; Sigma Aldrich) to induce TetO gene expression. From day 1 to day 7, puromycin (3 μg ml^{-1}; Thermo Fisher Scientific) was added to the culture medium for selection. On day 4, surviving neuronal progenitors were dissociated with StemPro Accutase cell dissociation reagent (Life Technologies) with DNase (0.1 mg ml^{-1}, Sigma Aldrich) and replated on poly-L-ornithine (0.1 mg ml^{-1}), laminin (10 μg ml^{-1}) and fibronectin (10 μg ml^{-1}; all from Sigma Aldrich) triple-coated plastic wells at a density of 91,000 cells per square centrimetre in the maturation medium, Neurobasal medium supplemented with B-27 2%, GlutaMAX supplement 1%, penicillin–streptomycin 0.5%, ascorbic acid (200 μM; Sigma Aldrich), DAPT (2.5 μM; Tocris) and doxycycline (1 μg ml^{-1}). On day 8, culture medium was replaced with fresh maturation medium without doxycycline. Cells were used for infection experiments on day 15.

Isolation of RNA from iPSC-derived cells

iPSC-derived brain cells were obtained from commercial sources (cortical neurons and astrocytes from Applied Stem Cell, microglia from Axol, and oligodendrocyte progenitor cells from Tempo Bioscience). The cells were thawed, pelleted and washed in ice-cold PBS, and total RNA was isolated using High Pure RNA isolation kit (Roche).

Expression of TMEFF1 in the adult human brain

Data on expression of TMEFF1 in the human brain were obtained from previously published single-nucleus RNA-sequencing data across the entire adult human brain[50]. The unique molecular identifier data from annotated cell types in the cerebral cortex were extracted and plotted.

CRISPR–Cas9-targeting of individual genes in neurons

Knockout of specific genes in HEK293T and SK-N-SH cells was achieved by CRISPR–Cas9 technology and in most cases verified by immunoblotting. Briefly, ribonucleoprotein complexes were made by complexing Cas9 and sgRNA at a molar ratio of 1:2.5 (Cas9/sgRNA) at 25 °C for 15 min before nucleoporation. Cells were resuspended in OptiMEM (Gibco, Thermo Fisher Scientific) and electroporated with a concentration of 300 μg ml^{-1} Cas9 protein using the Lonza 4D-Nucleofector System (program CM-138). To target *TMEFF1* and *SP100* in LUHMES cells and ESC-derived cortical neurons, we used lentivirus-delivered Cas9 and guide RNA. Briefly, guide RNAs targeting *TMEFF1* and *SP100*, were cloned into lenti-CRISPR v2 or plentiCRISPRv2 containing the blasticidin resistance gene[51] following Golden Gate assembly, as described previously[52] utilizing the Esp3I restriction site in plentiCRISPRv2. The used gRNAs are listed in Supplementary Table 2. For LUHMES cells, we transduced undifferentiated cells with lenti-CRISPR v2 containing TMEFF1 sgRNA1 or sgRNA2, or a control sgRNA (mouse ATG5) used as control. LUHMES cells were then differentiated into neurons and were selected 3 days later with 10 mg ml^{-1} blasticidin. For ESC-derived neurons, the lentivirus was delivered to differentiated cell cultures and selected with 10 mg ml^{-1} blasticidin for 3 days before use in experiments. Lentiviral vector production was carried out as previously described[53]. Briefly, lentiviral preparations were concentrated by ultracentrifugation and quantified by p24 ELISA (Xpress BioA). The hESC-derived neurons were cultured with Neurobasal medium containing 200 μmol ascorbic acid, 2.5 μmol DAPT, 2 μl ml^{-1} doxycycline and 3 μg ml^{-1} puromycin. The used gRNAs are listed in Supplementary Table 2.

Flow cytometry

HEK293T cells were washed with ice-cold PBS three times and digested with 0.05% trypsin (with EDTA); cells were collected by centrifugation for

3 min at 500*g*. Then cells were washed three times and incubated with 4% PFA for 30 min. For LUHMES- and hESC-derived neurons, cells were collected by 3 min incubation in PBS with 0.5 mM EDTA and 0.02% trypsin. The cells were then fixed by PFA 4% for 20 min at room temperature. After three washes in PBS, the cells were resuspended in FACS buffer (PBS 0.2 mM EDTA and 5% FCS), and GFP expression was measured on a NovoCyte 2100YB flow cytometer equipped with two lasers (488 nm and 561 nm) and ten detectors (Agilent). For primary mouse astrocyte and microglia cultures, cells were incubated for 20 min with anti-CD16/CD32 and Fixable Live/Dead Near-IR Dead Cell Stain (Thermo Fisher Scientific, catalogue number L10119), fixed using −20 °C cold methanol for 5 min, and stained with APC anti-mouse CD45 (Biolegend, catalogue number 103112), BV421 anti-mouse CD11b (Biolegend, catalogue number 101236) and AF488 anti-mouse GFAP (eBioscience, catalogue number 53-9892-82). The data generated were analysed using both the NovoExpress (v1.6.1, Agilent) and FlowJo v10.8.1 (BD Life Sciences) software programs. The gating strategy is shown in Supplementary Fig. 2.

LDH assay

For the LDH assay, 50 µl of supernatant was transferred to a new 96-well plate and 50 µl reaction buffer was added, followed by 30 min incubation protected from light. The reaction was read at wavelengths of 450 nm and 690 nm. To quantify LDH release, we used the formula: ($Sample_{LDH\ activity}$ − $Spontaneous_{LDH\ activity}$)/($Maximum_{LDH\ activity}$ − Spontaneous *LDH activity*)*100. Sample (OD, 450) = Output A450 − Blank A450.

Quantitative PCR with reverse transcription

Gene expression was determined by real-time quantitative PCR, using TaqMan detection systems (Applied Biosciences). RNA was extracted using the High Pure RNA isolation kit (Roche), and RNA quality was assessed by Nanodrop spectrometry (Thermo Fisher). Taqman assays for quantitative PCR were: *IFNB* (Hs01077958_s1), *MXA* (Hs00895608_m1), *CCL2* (Hs00234140_m1), *TMEFF1* (Hs00902905_m1), *NKX2-8* (Hs.234763), *CTXN1* (Hs.657978) and *ACTB* (Hs01060665), *Tmeff1* (Mm01345565_m1) and *Actb* (Mm00607939_s1) (Applied Bioscience).

Evaluation of HSV-1 entry

For evaluation in transfected HEK293T cells, the cells were seeded in 12-well plates with a coverslip 1 day before transfection (4×10^4 cells per well) with 2 µg plasmids per well (unless otherwise specified) using Lipofectamine 2000 (Thermo Fisher Scientific). Medium was changed 6 h post transfection to avoid toxicity. At 24 h post transfection, cells were infected with HSV-1 K26GFP at an MOI of 30. For evaluation in neurons, 2×10^5 LUHMES- and hESC-derived neurons were inoculated with either MOI 50 or MOI 20, representing 3×10^7 and 1.2×10^7 PFUs per millilitre, respectively. Cells were treated with acyclovir. Inoculation was carried out on ice in CO_2-independent medium complemented with 0.01% BSA for 1 h. Cells were then transferred to differentiation medium and incubated for 2 h at 37 °C with 5% CO_2. The cells were fixed in 4% PFA for 20 min at room temperature, permeabilized in PBS with 0.1% Triton X-100, and incubated for 30 min each at room temperature with primary antibodies to β3-tubulin (1:100; D1G9, Cell Signaling Technology) and ICP5 (1:200; ab6508, Abcam), followed by a second incubation with donkey anti-rabbit Alexa Fluor 568 and donkey anti-mouse Alexa Fluor 488 (Thermo Fisher Scientific), and DAPI (1:50,000; Thermo Fisher Scientific) in PBS with 0.5% BSA. After washing, slides were mounted with antifade solution (Beyotime Biotechnology) or in ProLong Gold (Thermo Fisher Scientific). Images were acquired using a Zeiss LSM 800 confocal fluorescence microscope or a Nikon A1Si laser scanning confocal microscope. Pseudo-colouring, brightness and contrast were adjusted identically across each set of images using ImageJ (FIJI). The quantification of HSV-1 capsids accumulating at each nucleus was carried out through an automated pipeline based on the CellProfiler software[54].

Cloning and expression of proteins

pCMV-TMEFF1 (WT, N- and C-terminal truncations and point mutations) and pCMV-MYH9/MYH10 were constructed by replacing the *eGFP* gene of pCMV-egfp with *TMEFF1*, *MYH9* or *MYH10*; pCMV-MYH9/MYH10–GFP1–10 were constructed by inserting GFP1–10 fragments on the N terminus of *MYH9*/*MYH10*; pCMV-TMEFF1-GFP11 was constructed by inserting the GFP11 fragment onto the C-terminal end of *TMEFF*; pCMV-TMEFF1-HA was constructed by tagging an HA tag on the N terminus of *TMEFF1*. Expression vectors for NKX2-8, CTXN1, nectin-1 and HVEM were on the pRP backbone and were obtained from Vectorbuilder.

Immunoblotting

For whole-cell lysates from HEK293T cells, cells were washed with ice-cold PBS three times and lysed with RIPA (50 mM Tris, 150 mM NaCl, 1% Triton X-100, 1% sodium deoxycholate, 0.1% SDS, pH 7.4) at 4 °C for 30 min. Supernatants were collected after centrifugation for 10 min at 4 °C and concentrations were determined with the BCA kit (Thermo Fisher Scientific). Lysates were added with 5× loading buffer and boiled for 5 min to denature them. Samples were separated by electrophoresis in 4–20% polyacrylamide gel electrophoresis (PAGE) gel and transferred to a 0.45-mm PVDF membrane. The blots were blocked for 1 h at room temperature in 5% non-fat milk (diluted in Tris-buffered saline (TBS) with 0.1% Tween 20), followed by incubation overnight at 4 °C in primary antibody. Membranes were washed three times and incubated with secondary antibody for 1 h at room temperature. After washing, chemiluminescent detection was carried out using an ECL kit (Thermo Fisher Scientific). The antibodies used were: anti-NMHC-IIA (Proteintech; 11128-1-AP; 1:2,000); anti-NMHC-IIB (Proteintech; 21403-1-AP; 1:2,000); anti-nectin-1 (Proteintech; 24713-1-AP; 1:250); anti-TMEFF1 (Santa Cruz; sc-393457; 1:500); anti-Flag (Proteintech; 66008-4-Ig; 1:5,000); anti-HA (Proteintech; 66006-2-Ig; 1:10,000); anti-vinculin (Sigma Aldrich; V9131; 1:1,000); anti-VP5 (Santa Cruz; sc-56989; 1:500); anti-HVEM (Santa Cruz; sc-365971; 1:100); anti-MAG (Cell Signaling; 9043; 1:400); anti-PILRα (Novus Biological; DDX0230P-100; 1:100); anti-GST (Abmart; M20025; 1:5,000); anti-actin (Proteintech; HRP-60008; 1:5,000).

Immunoprecipitation

HEK293T cells were seeded in 10-cm dishes (2×10^6 cells). One day later, 13 µg plasmids was transfected per dish using calcium phosphate. The medium was changed 6 h later. HSV-1-GFP was added and maintained for 17 h at an MOI of 15. Cells were washed with ice-cold PBS three times and lysed with lysis buffer (50 mM Tris, 150 mM NaCl, 1 mM EDTA, 1% Triton X-100, 1.5 mM Na_3VO_4, 50 mM NaF, 10 mM sodium pyrophosphate, 10 mM sodium beta-glycerophosphate, 1× protease inhibitor cocktail, pH 7.4) for 30 min at 4 °C. Supernatants were collected after centrifugation for 10 min at 4 °C and concentrations were then determined with the BCA kit. A 1 mg quantity of protein lysate was used per reaction together with 1 µg antibody and 20 µl protein G beads. The mixtures were incubated at 4 °C with rotation overnight. Beads were collected and washed with ice-cold PBST (0.2% Tween 20) three times (15 min for each time). After washing, beads were boiled with 5× loading buffer to denature the proteins, which were then subjected to SDS–PAGE.

Electron microscopy

Transmission electron microscopy was carried out with a 120-kV biology transmission electron microscope (Tecnai G2 SpiritBiotwin, Shanghai Jiao Tong University). The samples for biological transmission electron microscopy were stained on copper TEM grids (3.05 mm; 200 mesh, Beijing Zhongjingkeyi Technology). A 10-µl sample was dropped on the grids and stained for 1–3 min. Then, 10 µl of 2% uranyl acetate solution was used to stain the grid for 10 min. The excess solution was wicked

off by blotting the grid at a 45° angle with filter paper. The grid was stored in the dark in the Petri dish at room temperature until imaging.

Mass spectrometry

Samples were loaded on 4–20% PAGE gel for separation, and the gel was developed with Fast Silver Stain Kit (Beyotime Biotechnology). Targeted bands were cut and treated for in-gel digestion. The extracted material was analysed by nanolitre liquid chromatography–mass spectrometry (Easy nLC1200/Q Exactive plus, Thermo Fisher Scientific). Data were analysed by Peaks Studio10.0 software and the sequences were aligned with human herpesvirus and *Homo sapiens* databases.

Quantification of viral load

HSV-1 genomes were quantified by PCR. Briefly, DNA was isolated from either total cells or cellular fractions as indicated in the figure legends using QIAamp Fast DNA Tissue Kit or phenol–chloroform. The viral DNA was amplified by PCR using the following primers: 5′-CGCATCAAGACCACCTCCTC-3′ (HSV-1 gB, forward), 5′-AGCTTGCGG GCCTCGTT-3′ (HSV-1 gB, reverse) and 5′-CGGCCCAACATATCGTTGA CATGGC-3′ (HSV-1 gB, probe). For quantification of HSV-1 and HSV-2 infectious particles, we used Vero cell-based plaque assays as described previously[55]. VZV replication was determined by measurement of the viral *ORF63* transcript[56], whereas poliovirus replication was evaluated by a $TCID_{50}$ assay on HeLa cells[44]. For quantification of virus from mouse organs, samples were prepared from the brainstem and trigeminal ganglion homogenates, and centrifuged for 10 min at 3,000*g* (precooled at 4 °C to pellet cellular debris).

GST pull-down

For GST pull-down, the C terminus of *TMEFF1* was cloned into pGEX-4T1 and transformed into BL21 Star (DE3) for protein expression. *Escherichia coli* precipitates were collected and purified with GST-tag Protein Purification Kit (Beyotime Biotechnology). HEK293T cells were lysed with lysis buffer (50 mM Tris, 150 mM NaCl, 1 mM EDTA, 1% Triton X-100, 1.5 mM Na_3VO_4, 50 mM NaF, 10 mM sodium pyrophosphate, 10 mM sodium β-glycerophosphate, 1× protease inhibitor cocktail, pH 7.4) and incubated with 100 μg purified protein as well as glutathione beads. The mixtures were incubated at 4 °C with rotation overnight. Beads were collected and washed with ice-cold PBST (0.2% Tween 20) three times (15 min for each time). Loading buffer was added to the beads, and the beads were boiled for 5 min to denature the proteins.

Surface plasmon resonance

To isolate pure proteins, TMEFF1-C was inserted into the pGEX-4T1 vector, which was digested by Sal1 and Not1. TMEFF1-C–GST was expressed in *E. coli* strain BL21(DE3) and purified with anti-GST beads. pCMV-IIA-CC-HA was constructed by replacing the GFP gene in the pCMV-eGFP vector with IIA-CC–HA. IIA-CC–HA was expressed with HEK293T cells and purified with anti-HA beads. All samples prepared for surface plasmon resonance were desalted with a desalting column (Thermo Fisher Scientific, Zeba) and diluted in HBS-EP buffer (10 mM HEPES pH 7.4, 150 mM NaCl, 3 mM EDTA, 0.005% Tween 20). The binding affinity between TMEFF1-C–GST and IIA-CC–HA was measured by a Biacore 8K (Cytiva). HA peptide did not show binding to TMEFF1-C, and was used as a reference. TMEFF1-C–GST was diluted with 10 mM glycine HCl (pH 5.0) at a concentration of 2 μg ml^{-1} and then immobilized on a CM5 sensor chip. IIA-CC–HA was diluted with HBS-EP buffer at an increasing concentration ranging from 12.5 μg ml^{-1} to 200 μg ml^{-1}. Running buffer for the assay was HBS-EP buffer. Data were analysed with Biacore Insight Evaluation Software 4.0.12.15655.

Split GFP

The split GFP system was constructed by fusing TMEFF1, and SARS-CoV-2 spike, to GFP11, and by fusing NMHC-IIA, NMHC-IIB and nectin-1 to GFP1–10 domain. For the split GFP assay, HEK293T cells were seeded in a 12-well plate 1 day before transfection (2×10^5 cells per well); 2 μg plasmids (1 μg for each plasmid) was transfected in each well. Cells were collected 48 h post transfection for detection.

AlphaFold

The structures of protein complexes were predicted using a local installation of AlphaFold[57], and the AlphaFold-Multimer version optimized for complexes[58]. The predicted alignment scores from the AlphaFold runs were extracted using AlphaPickle. All output models were manually inspected and evaluated for meaningfulness and complexes with high predicted aligned error (PAE) scores between chains were discarded. For studies of the effects of alterations, interface residues targeted for substitution were selected on the basis of inter-distances (<4 Å) and chemistry. Prediction of the structure of the human TMEFF1–NMHC-II complex by AlphaFold using the full-length protein sequences proved difficult owing to the high number of disordered regions; thus, we used the TMEFF1 (UniProt Q8IYR6, isoform 1) C-terminal domain residues 352–380 and NMHC-IIA (UniProt P35579) CC domain residues 837–1926. One output model predicted an interaction between TMEFF1 and NMHC-II, which also reflected in the low PAE scores between the two chains. Similarly for prediction of the structure of the human TMEFF1–nectin-1 complex, the AlphaFold prediction with full-length protein sequences was not successful; thus, we used TMEFF1 residues 40–321 and nectin-1 (UniProt Q15223, isoform 1) ectodomain residues 31–338. Here all output models showed interactions of the two chains; however, model 1 showed the lowest PAE scores between the two chains and thus was used for analysis of probable interacting residues. Protein structure figures were generated using ChimeraX.

Peptides

The TMEFF1-C peptide corresponding to the C-terminal domain of TMEFF1 fused to the HIV-Tat cell permeability peptide had the sequence H-YGRKKRRQRRRTRKCPKNNRGRRQKQNLGHFTSDTSSRMV-OH. We used HIV-Tat (YGRKKRRQRRR) and HA (YPYDVPDYA) as control peptides. The peptides were obtained from Schafer-N.

Validation of *Tmeff1*$^{-/-}$ mice

Animals were genotyped by extraction of genomic DNA from tails. At weaning, 3 weeks of age, 2 mm of the tail was cut and digested overnight at 55 °C in 500 μl PBS + 0.5% SDS, 1 mg ml^{-1} Proteinase-K, 10 mM EDTA, 0.4 M NaCl, 0.2 M Tris-HCl. DNA was isolated by NaCl (5 M) and isopropanol centrifugation, and analysed by PCR and Sanger sequencing.

For PCR, we used DreamTaq PCR Mastermix (Thermo Fisher Scientific), and 1 μg DNA was amplified using TMEFF1 primers (see sequences below). After a hot start at 95 °C for 5 min, 35 cycles were run accordingly: 30 s at 95 °C, 1 min at 60 °C and 1 min at 72 °C. The genotype was visualized by running the PCR product on a 2% agarose gel at 90 V for 30 min. The primers used were: Pr1 (common - forward), 5′-CCAAGATGTCCTCCAGGCGAGTTAG-3′; Pr2 (WT - reverse), 5′-GGATCCTTCTCTCTGGTGCCTTTG-3′; Pr3 (knockout, LTR - reverse), 5′-AAATGGCGTTACTTAAGCTAGCTTGC-3′ (all from LGC Biosearch Technologies).

For Sanger sequencing, DNA was extracted from 2% agarose gel using the Monarch DNA gel extraction kit (New England BioLabs) and eluted in 17 μl. A 15 μl volume of the extracted DNA was added to 2 μl of 10 μM Pr1 primer, and commercially sequenced using the LightRun modality from Eurofins Genomics. Sanger sequencing data were analysed using SnapGene software.

Tmeff1 mRNA expression in the brains from WT and *Tmeff1*$^{-/-}$ mice was evaluated by quantitative PCR with reverse transcription. Mice were anaesthetized with isoflurane and euthanized by decapitation. Brains were dissected and the cortex, hypothalamus, brainstem, cerebellum, olfactory bulb and spinal cord were isolated for expression analysis. The brain tissue was added to 200–500 μl DPBS (Sigma Aldrich), and homogenized using one 3-mm tungsten carbide bead (Qiagen) per

sample for 3 min, frequency of 30 shakes per second in a TissueLyzer II (Qiagen). An 80 µl volume of tissue homogenate was used for RNA extraction using a High Pure RNA isolation kit (Roche). RNA concentration was measured using a NanoDrop spectrophotometer. A 45 ng quantity of RNA in technical duplicates was used in the TaqMan Gene expression assays.

HSV-1 CNS infection in mice

TMEFF1-deficient mice generated with the gene trap approach were obtained from Taconic. The mice were available as a cryopreserved line as 129/SvEv-C57BL/6N hybrid embryos and reconstituted onto a C57BL/6N background. When bred as heterozygous × heterozygous (on a mixed background), they generated offspring in Mendelian ratios, and *Tmeff1*$^{+/+}$ WT littermates were used as controls for experiments. Both female and male animals were used. To model HSE-like disease in mice, we used an ocular HSV-1 infection route[27], to mimic the natural epithelial route of infection and HSV-1 entry into the CNS by retrograde transport via the trigeminal ganglia. In short, age-matched (6–8 weeks), WT and *Tmeff1*$^{-/-}$ littermates, female and male mice, were anaesthetized by intraperitoneal injection of ketamine (100 mg kg^{-1} body weight) and xylazine (10 mg kg^{-1} body weight). Using a 29-G syringe, corneas were scarified in a 10 × 10 cross pattern and mice were inoculated with 2×10^6 PFUs HSV-1 (McKrae) in 5 µl per eye. Mice were treated with infection medium (DMEM + 2% penicillin–streptomycin), or mock infected with 5 µl per eye of infection medium without virus. For select experiments, WT C57BL/6N mice received TMEFF1-C, HIV-Tat or scrambled peptide (8 µl, 80 µM) or acyclovir (8 µl, 40 µM) twice per day applied to the cornea, and were infected in the cornea with HSV-1 (2.6×10^6 PFUs per eye). Mice were monitored daily for weight loss and development of symptoms. Disease symptoms were scored according to previously published descriptions in a blinded manner[27], with the following minor modifications. In short: eye irritation (0: none; 1: watering eyes, slight swelling of the lids; 2: secretion (pus), moderate swelling, moderate periocular hair loss; 3: severe hair loss limited to periocular, severe swelling, eye completely shut); head swelling (0: none; 1: minor swelling, slight distortion of facial symmetry; 2: moderate swelling, creating a palpable bump on the forehead; 3: severe swelling, large palpable bump on forehead, often diffused to eyes and between ears); neurological symptoms (0: normal; 1: jumpy; 2: uncoordinated, ruffled fur; 3: hunched back and/or lethargic). Mice were euthanized at day 5 post infection or if humane endpoints were met, including weight loss >25% of the starting weight, skin lesions at the eyes or head swelling, severe lethargy, shaking or unresponsiveness. For survival studies, mice were followed until reaching a humane endpoint or 100% of the starting weight. Survival studies were repeated on *Tmeff1*$^{-/-}$ mice fully backcrossed onto the C57BL/6N background for ten generations. Statistical methods were not used to determine sample size.

Isolation and culture of brain cell types from newborn mice

Primary CNS cells were isolated from whole brains of mice postnatal day 0–3 using the Neural Tissue Dissociation Kit (MACS, Miltenyi Biotec) according to the manufacturer's instructions. The dissociated cells were plated for 60 min in T175 culture flasks to isolate the quickly attaching non-neuronal cell fraction, including microglia and astrocytes, after which the neuron-containing non-attached cell fraction was collected and plated separately. The cells of the neuron-containing cell fraction were seeded on 48-well plates pre-coated with poly-L-lysine (Sigma Aldrich) and laminin (Invitrogen) at a density of 2×10^5 cells per well. The cells were cultured in Neurobasal-A medium (Gibco) containing 2% B-27 supplement (Gibco), 2 mM L-glutamine (Gibco), 100 mg ml^{-1} Primocin (Invivogen). In addition, 20 mM floxuridine + 20 mM uridine (Sigma Aldrich) was added to kill any dividing cells and leave only the non-dividing neurons. Medium was changed every third day. On day 10, the purity of the neuron cultures was assessed by flow cytometry. The cells of the quickly attaching cell fraction were split into two fractions, and one was cultured for microglia enrichment and one was cultured for astrocyte enrichment. Both fractions were cultured in DMEM + 10% FBS supplemented with 2 mM L-glutamine and 1% penicillin–streptomycin. Astrocyte enrichment was achieved according to a previously published method[27] by splitting the cultures with 0.5% trypsin + 0.5 mM EDTA at a ratio of 1:4 once per week for 4 weeks, selecting for the faster growing astrocytes (and depletion of slower growing microglia).

Microglia enrichment was achieved according to a previously published method[59]. In short, the confluent mixed glial cells were cultured for 4 weeks, without splitting the culture, and the medium was changed once per week, resulting in microglia growth with layered astrocytes on top. The astrocyte layer growing above the microglia was removed using mild trypsinization (0.05–0.12% trypsin in DMEM) for 30 min. The remaining strongly adherent microglia were isolated by subsequent trypsinization using 0.5% trypsin + 0.5 mM EDTA. The purity of enriched primary CNS cell cultures was assessed by flow cytometry as previously reported[27]. Primary CNS cells (astrocytes, microglia and neurons) were plated at 2×10^5 cells per well in 48-well plates and used for experiments.

Immunohistochemistry

Animals were anaesthetized and perfused through the left ventricle (and draining from the right atrium) with 20 ml DPBS followed by 20 ml 10% formalin solution (Sigma Aldrich). The perfusion-fixed brains were dissected out and transferred to 10% formalin for continued fixation for 24 h. Formalin-fixed brains were paraffin-embedded (FFPE) in histology blocks. FFPE tissue blocks were cut into slides of 8 µm using an SLEE microtome (SLEE Medical) and transferred to Superfrost Plus Microscope slides (Thermo Scientific). FFPE slides were rehydrated by heating for 30 min at 60 °C following rapid transfer to a xylene bath for 2 × 5 min. The rehydration followed incubation for 2 × 5 min in decreasing concentrations of ethanol, from 99% to 96% to 70%. After the last incubation with ethanol, the slides were washed under running demineralized water for 5 min. The rehydrated slides were soaked in prewarmed (80 °C) Dako antibody target retrieval buffer (Dako) and incubated at 80 °C for 30 min, followed by two washes in cold DPBS, and cold blocking of endogenous peroxidase using 10% methanol for 15 min on ice. Slides were washed 2 × 5 min in PBS, followed by one rinse for 10 min in TBS + 0.3% Tween20 (TBS-T) + 1% BSA (Sigma Aldrich). Slides were incubated with polyclonal rabbit anti-HSV (Dako), and monoclonal mouse anti-NeuN (Merck Millipore) or monoclonal mouse anti-S100 (Abcam) at 1:300 dilution in DPBS + 1% BSA, at 4 °C overnight in a humidified chamber. The next day, slides were tempered for 1 h at room temperature, followed by rinsing 3 × 3 ml per slide with TBS-T + 0.2% BSA. Slides were incubated for 1 h at room temperature with Alexa Fluor 568-conjugated secondary donkey anti-mouse or Alexa Fluor 488 donkey anti-rabbit IgG (Thermo Fisher Scientific) diluted 1:500 in TBS-T + 1% BSA. Slides were finally washed 3 × 3 ml per slide with TBS-T + 0.2% BSA followed by soaking for 10 min in PBS. Cover glasses were mounted using 10 µl Prolong Gold with DAPI (Thermo Fisher Scientific). Slides were imaged using a Zeiss LSM 800 Airyscan Laser scanning confocal microscope. Both the right and left side of the brainstem (WT $n = 4$, *Tmeff1*$^{-/-}$ $n = 5$) at three different anatomic bregmata (coronal plate, −5.80, −6.72, −7.20 mm) were imaged at ×10 and ×40. Only images containing HSV-1 foci were quantified. In short, all HSV-1$^+$ cells were counted per image, followed by counting of all HSV-1$^+$ cells co-localizing with NeuN$^+$ or S100$^+$ cells. Additionally, outliers were identified and excluded using a Rout analysis with $Q = 1$

Study approval

All animal experiments were approved in advance by the respective local authorities—Aarhus: Animal Ethics Committee at the Danish Veterinary and Food Administration (permission number 2016-15-0201-01085); Shanghai: Shanghai Jiao Tong University Laboratory Animal Ethics and Use Committee (Shanghai permission number 201902035).

All experiments were carried out in accordance with local regulations (that is, Danish Animal Welfare Act for the Care and Use of Animals for Scientific Purposes; Institutional Animal Care and Use Committee of Shanghai Jiao Tong University, China).

Statistical analyses and reproducibility

The data are shown as means of biological replicates ± s.d. The sample number (n) indicates the number of cellular experiment repeats, mice or cells included in quantification, as specified in the figure legends. Statistically significant differences between two groups were determined using two-tailed unpaired t-tests for data exhibiting normal distribution, or a two-tailed Mann–Whitney U-test when analysing data that did not pass the normal distribution test. For multiple comparisons with one or more variables, a two-tailed one-way ANOVA or two-way ANOVA test was applied, respectively. When finding that the difference in the mean between groups were significantly different in the ANOVA, a subsequent two-tailed unpaired t-test was carried out comparing groups of interest. All comparisons are indicated with P values shown. For analysis of survival data, we used the log-rank Mantel–Cox test, and mixed-effect analysis with Geisser–Greenhouse correction was used for analyses of disease progression comparing changes between genotypes over time. The data shown are representative data from single experiments with three or more biological replicates, unless otherwise stated in the figure legends. The experiments were carried out at least three times with similar results, unless otherwise stated in the figure legends.

Reporting summary

Further information on research design is available in the Nature Portfolio Reporting Summary linked to this article.

Data availability

All data supporting the findings of this study are available in the paper and its Supplementary Information. Sequencing data from the CRISPR screens are available in the Gene Expression Omnibus (accession number GSE268182). Source data are provided with this paper.

45. Rosato, P. C. et al. Neuronal IFN signaling is dispensable for the establishment of HSV-1 latency. *Virology* **497**, 323–327 (2016).
46. Cai, W. Z., Person, S., Warner, S. C., Zhou, J. H. & DeLuca, N. A. Linker-insertion nonsense and restriction-site deletion mutations of the gB glycoprotein gene of herpes simplex virus type 1. *J. Virol.* **61**, 714–721 (1987).
47. Ligas, M. W. & Johnson, D. C. A herpes simplex virus mutant in which glycoprotein D sequences are replaced by beta-galactosidase sequences binds to but is unable to penetrate into cells. *J. Virol.* **62**, 1486–1494 (1988).
48. Szpara, M. Isolation of herpes simplex virus nucleocapsid DNA. *Methods Mol. Biol.* **1144**, 31–41 (2014).
49. Chen, M. et al. Rapid generation of regionally specified CNS neurons by sequential patterning and conversion of human induced pluripotent stem cells. *Stem Cell Res.* **48**, 101945 (2020).
50. Siletti, K. et al. Transcriptomic diversity of cell types across the adult human brain. *Science* **382**, eadd7046 (2023).
51. Sanjana, N. E., Shalem, O. & Zhang, F. Improved vectors and genome-wide libraries for CRISPR screening. *Nat. Methods* **11**, 783–784 (2014).
52. Neldeborg, S., Lin, L., Stougaard, M. & Luo, Y. Rapid and efficient gene deletion by CRISPR/Cas9. *Methods Mol. Biol.* **1961**, 233–247 (2019).
53. Ryo, L. B., Thomsen, E. A. & Mikkelsen, J. G. Production and validation of lentiviral vectors for CRISPR/Cas9 delivery. *Methods Mol. Biol.* **1961**, 93–109 (2019).
54. Dohner, K. et al. Importin alpha1 is required for nuclear import of herpes simplex virus proteins and capsid assembly in fibroblasts and neurons. *PLoS Pathog.* **14**, e1006823 (2018).
55. Reinert, L. S. et al. Brain immune cells undergo cGAS-STING-dependent apoptosis during herpes simplex virus type 1 infection to limit type I interferon production. *J. Clin. Invest.* **131**, e136824 (2021).
56. Ogunjimi, B. et al. Inborn errors in RNA polymerase III underlie severe varicella zoster virus infections. *J. Clin. Investig.* **127**, 3543–3556 (2017).
57. Jumper, J. et al. Highly accurate protein structure prediction with AlphaFold. *Nature* **596**, 583–589 (2021).
58. Abramson J. et al. Accurate structure prediction of biomolecular interactions with AlphaFold 3. *Nature* **630**, 493–500 (2024).
59. Saura, J., Tusell, J. M. & Serratosa, J. High-yield isolation of murine microglia by mild trypsinization. *Glia* **44**, 183–189 (2003).

Acknowledgements S.R.P. was supported by the European Research Council (786602), the Novo Nordisk Foundation (NNF18OC0030274 and NNF20OC0064301), the Lundbeck Foundation (R359-2020-2287), the Danish National Research Foundation (DNRF164) and the Swedish Research Council (2021-00942). Y.C. was supported by the National Natural Science Foundation of China (31971364 and 32370148), the National Key R&D Program of China (2022YFC3400205) and the Shanghai Jiao Tong University Scientific and Technological Innovation Funds Key forward-looking layout fund from Shanghai Jiao Tong University (number AF4150049). M.I. received funding from the Carlsberg Foundation (CF17-0687) and the Lundbeck Foundation (R251-2017-1124). T.H.M. was supported by the Independent Research Fund Denmark (0134-00006B), the Novo Nordisk Foundation (NNF21OC0067157 and NNF20OC0064890) and the Lundbeck Foundation (R268-2016-3927). M.D. was supported by the Lundbeck Foundation (DANDRITE-R248-2016-2518). J.G.M. was supported by the Independent Research Fund Denmark (9039-00173B), the Novo Nordisk Foundation (NNF17OC0029042) and the Carlsberg Foundation (CF21-0363). P.N. was supported by the Lundbeck Foundation (R310-2018-3713). AlphaFold calculations were carried out on a computer cluster established with support from the Department of Molecular Biology and Genetics, Aarhus University, and the Danish Research Agency through the Danish national research infrastructure for cryo-electron microscopy (EMBION 5072-00025B). The flow cytometry experiments carried out at Aarhus University were conducted at the FACS core facility.

Author contributions The study was conceived and designed by Y.C. and S.R.P. Cell experiments were designed, carried out and analysed by Y.D., M.I., M.C.S., X.P., E.A.T., R.N., M.M., X.Q., M.B.I., L.S.R., R.K.F., M.C., M.E.C.-T., X.D., B.-c.Z., Q.L., Z.J., Y.Z., S.Z., L.D., J.Z. and Y.C. (while he was a post-doctoral researcher at Aarhus university where TMEFF1 was identified). Animal experiments were designed, carried out and analysed by M.I. Data were analysed and interpreted by Y.D., M.I., P.N., T.H.M., J.G.M., S.-Y.Z., J.-L.C., Y.C. and S.R.P. Funding was acquired by M.I., M.D., T.H.M., J.G.M., Y.C. and S.R.P. The manuscript was drafted by Y.C. and S.R.P., and edited by all authors, who support the conclusions.

Competing interests The authors declare no competing interests.

Additional information

Supplementary information The online version contains supplementary material available at https://doi.org/10.1038/s41586-024-07670-z.

Correspondence and requests for materials should be addressed to Yujia Cai or Søren R. Paludan.

Peer review information *Nature* thanks the anonymous reviewers for their contribution to the peer review of this work. Peer reviewer reports are available.

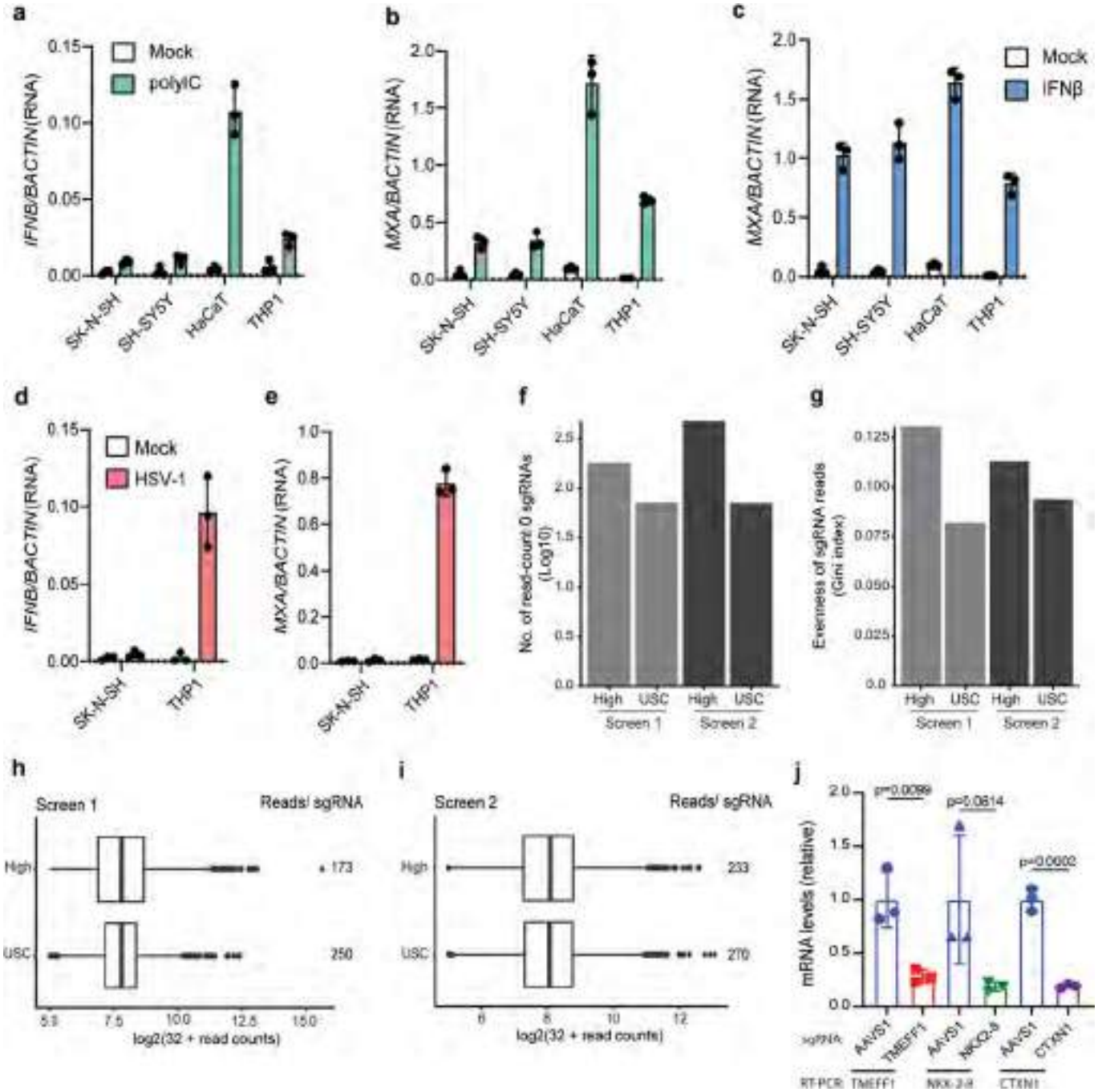

Extended Data Fig. 1 | Characterization of SK-N-SH cells and genome-wide CRISPR library fitness parameters. a-b, SK-N-SH, SH-SY5Y, HaCaT, and THP1 cells were stimulated with polyIC in the culture medium (25 µg/mL) for 6 h, and total RNA was isolated for analysis of *IFNB* and *MXA* transcripts by RT-qPCR (n = 3 biological replicates). **c**, SK-N-SH, SH-SY5Y, HaCaT, and THP1 cells were stimulated with IFNβ (25 ng/mL) for 6 h, and total RNA was isolated for analysis of *MXA* transcripts by RT-qPCR (n = 3 biological replicates). **d-e**, SK-N-SH, and THP1 cells were infected with HSV-1 (MOI 1) for 8 h, and total RNA was isolated for analysis of *IFNB* and *MXA* transcripts by RT-qPCR (n = 3 biological replicates). **f**, The number of sgRNAs with zero read counts following mapping and quantification with MAGeCK, displayed as log10 (number of zero read count sgRNAs) for each sample in the screens (n = 2 independent screens). **g**, Gini index of each sample as a measurement of the sgRNA read count distribution. **h-i**, Boxplot visualization of sgRNA read counts from mock and GFP^{high} samples of each screen. Q1 (25th percentile), median, Q3 (75th percentile); Whiskers defines as minima Q1 −1.5* interquartile range and maxima Q3 + 1.5* interquartile range. The sgRNA read count average/depth is denoted for each sample. USC, unsorted controls. **j**, SK-N-SH cells were treated with Cas9-gRNA RNPs targeting *TMEFF1*, *NKX2-8*, *CTXN1*, or *AAVS1*. Total RNA was isolated 36 h later, and levels of *TMEFF1*, *NKX2-8*, and *CTXN1* mRNA expression relative to *AAVS1* controls were determined by RT-qPCR (n = 3 biological replicates). Expression of mRNA transcripts was measured by RT-qPCR (a-e + j) and data is represented as means ± s.d. and analysed using unpaired two-tailed t-test; exact P-value shown. Data are representative of 3 independent experiments.

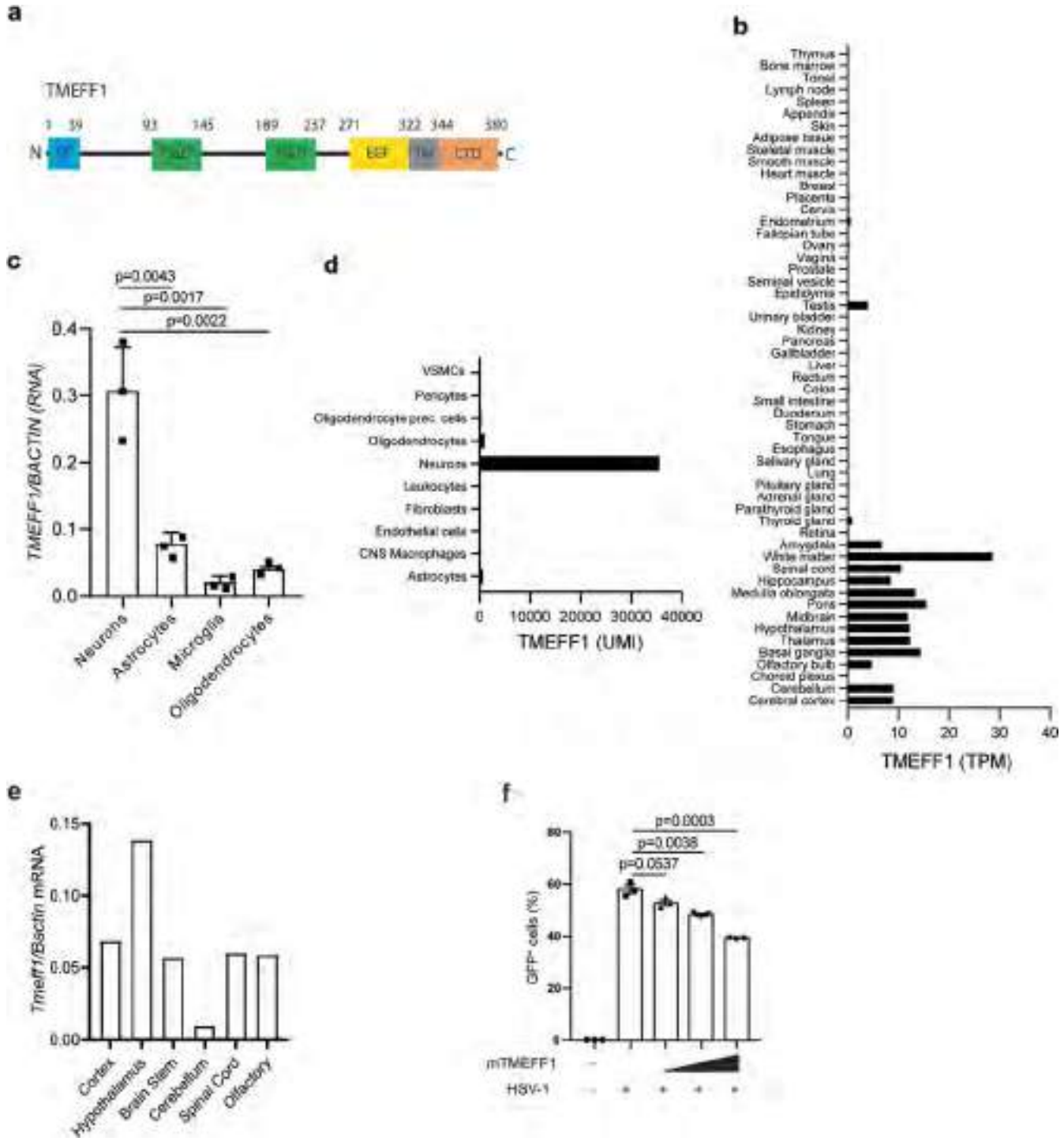

Extended Data Fig. 2 | Expression of TMEFF1 in tissues and CNS cell types. **a**, Domain structure of the TMEFF1 protein. A transmembrane protein with an EGF-like and two Follistatin-like domains in the extracellular region, a transmembrane region, and a cytoplasmic domain of unknown structure. SP signal peptide; FSLD: follistatin-like domain; EGF, EGF-like domain; TM, transmembrane domain; CTD, cytoplasmic domain. **b**, Expression of *TMEFF1* mRNA in different human tissues. TPM, transcripts per million. The graph is based on publically available data from Proteinatlas.org (date of data retrieval: August 1, 2022). **c**, Expression of *TMEFF1* mRNA relative to *BACTIN* in different cells representing cell types found in the human brain. Total RNA from iPSC-derived cortical neurons, astrocytes, microglia, and oligodendrocyte progenitor cells was analyzed for expression of *TMEFF1* mRNA by RT-qPCR (n = 2). **d**, UMI data on *TMEFF1* transcripts in annotated cell types in the cerebral cortex from previously published single-nucleus RNA sequencing data (ref. 50). VSMCs, Vascular smooth muscle cells. **e**, Total RNA was isolated from different regions of C57BL/6 mouse brain (n = 1), analyzed for *Tmeff1* mRNA levels by RT-qPCR. Data were normalized against *Bactin*. **f**, HEK293T cells were transfected with increasing amounts of mouse *Tmeff1* expression plasmid and infected with HSV-1-GFP. Percentage of GFP-positive cells was evaluated 12 h p.i (n = 3). Data are shown as means of biological sample replicates ± s.d. Statistical analysis was performed using a two-tailed one-way ANOVA test followed by unpaired t-tests of means indicated by P-values (c + e). $P < 0.05$ was considered statistically significant.

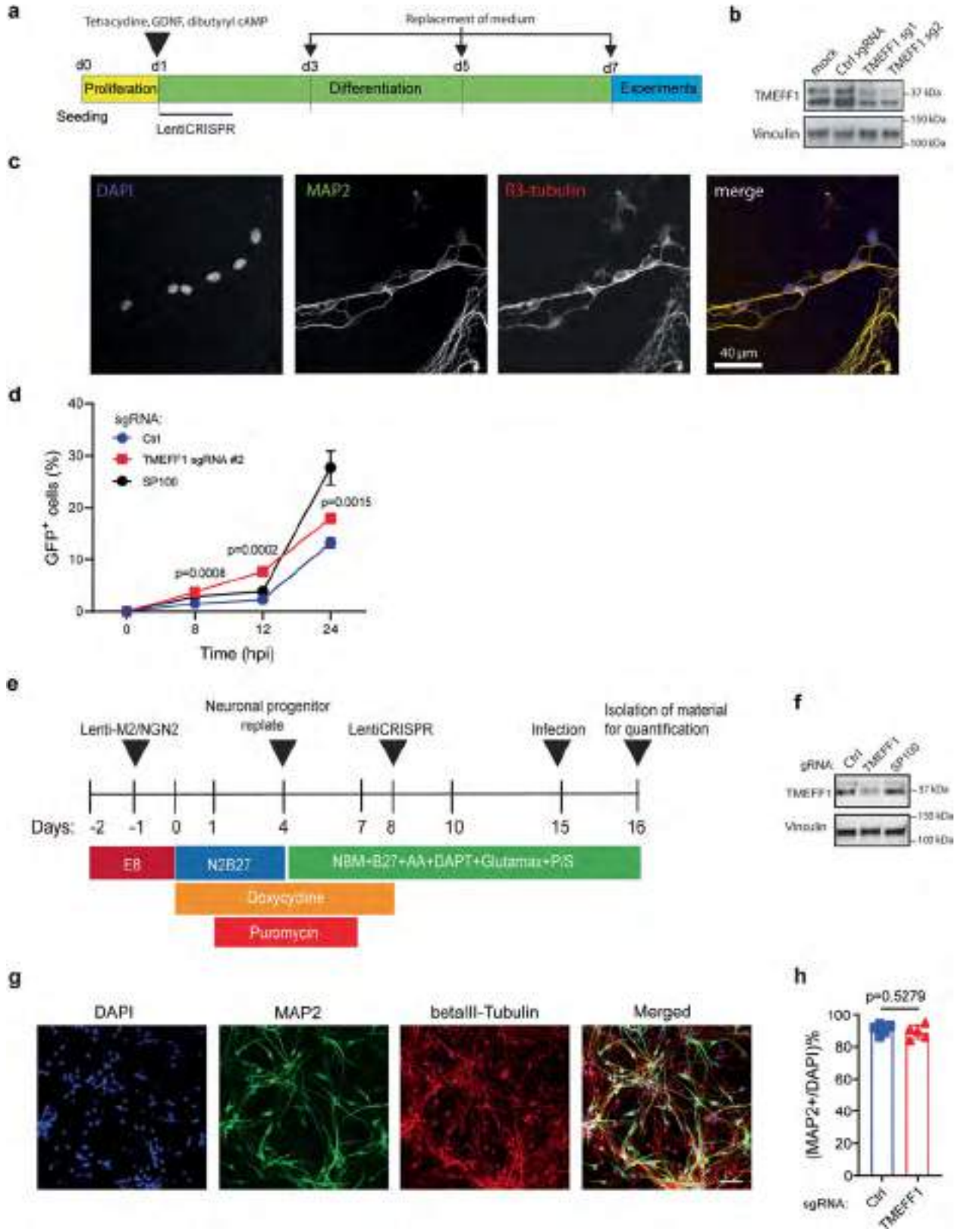

Extended Data Fig. 3 | See next page for caption.

Extended Data Fig. 3 | Generation of LUHMES- and stem cell derived neurons. **a**, Schematic illustration of the protocol for generation of LUHMES-derived neuron-like cells. **b**, Immunoblotting for TMEFF1 and vinculin in LUHMES neurons and effect of TMEFF1 sgRNA treatment. **c**, Confocal microscopy image of differentiated neurons stained with MAP2, betaIII-Tubulin, and DAPI, following the protocol shown in panel a (n = 3). **d**, LUHMES-derived neurons treated with TMEFF1 sgRNA #2 (Fig. 2b: TMEFF1 sgRNA #1) and infected with HSV-1-K64GFP (MOI 5) (n = 3 biological replicates pr time point). Cells were isolated after 8, 12, and 24 h, and examined by flow cytometry for GFP^+ signal. Data are presented as % GFP^+ cells. Two-tailed two-way ANOVA test followed by unpaired t-test comparing ctrl. with TMEFF1 sgRNA #2, comparing means, ±s.d. indicated by exact P-values (d).; $P < 0.05$ was considered statistically significant. **e**, Schematic illustration of the protocol for generation of ESC-derived cortical neurons. **f**, Immunoblotting for TMEFF1 in hESC-derived neurons and effect of TMEFF1 sgRNA treatment. **g**, Confocal microscopy image of differentiated neurons stained with MAP2, betaIII-Tubulin, and DAPI, following the protocol shown in panel e. Scale bar, 50 µm. **h**, Percentage of MAP2-positive cells, normalized to DAPI, in control and TMEFF1 sgRNA-transfected hESC-derived neurons. Immunoblots (b + f) and confocal imaging data (g) are representative of at least 3 independent experiments. Data is represented as mean ± s.d. (n = 5 biological replicates), and analysed using an unpaired two-tailed t-test. Exact P-values shown. P-values < 0.5 were considered significant. For gel source data, see Supplementary Fig. 1.

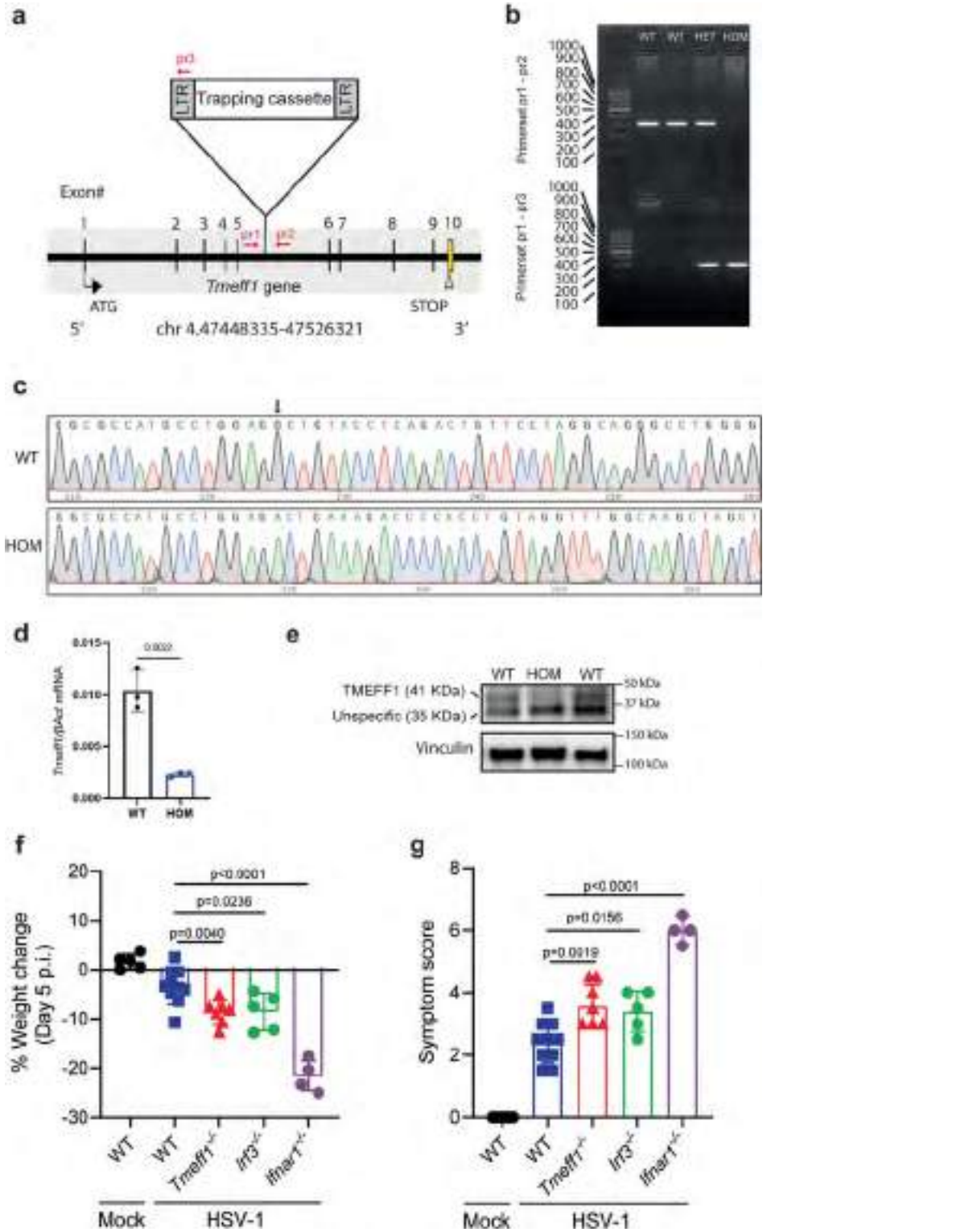

Extended Data Fig. 4 | Generation and characterization of *Tmeff1*$^{-/-}$ mice. **a**, Illustration of the targeting region of the gene trapping cassette used to generate *Tmeff1*$^{-/-}$ mice. The arrows in red represent the primers used for analysis og mouse genotypes. **b**, PCR analysis of DNA from *Tmeff1*$^{+/+}$ (WT), *Tmeff1*$^{+/-}$ (HET), and *Tmeff1*$^{-/-}$ (HOM) mice (littermates) using the primers pairs 1 and 2 *versus* 1 and 3 (Gel image representative of the standard genotyping of all HET x HET litters). **c**, Genomic sequences from WT and HOM mice around the genomic region targeted by the gene trapping cassette. **d**, Total RNA was isolated from the brains of C57BL/6N and HOM mice, analyzed for *Tmeff1* mRNA levels by RT-qPCR. Data were normalized against *Bactin* levels (n = 3 mice / genotype). Tmeff1 expression in WT and HOM mice were compared using an unpaired two-tailed t-test. P < 0.05 was considered significant. **e**, Brain lysates from WT and HOM mice were immunoblotted for TMEFF1 (representative of 2 individual repeats). **f-g**, WT, *Irf3*$^{-/-}$, *Ifnar1*$^{-/-}$, and *Tmeff1*$^{-/-}$ mice were infected in the cornea with 2×10^6 PFU/eye HSV-1 (Mckrae) and monitored for **f**, Weight change (day 5 p.i.), and **g**, Disease symptoms (day 5 p.i.). Each dot represents one animal (Mock infected, WT n = 5; Infected WT n = 12, *Tmeff1*$^{-/-}$ n = 7, *Irf3*$^{-/-}$ n = 5, *Ifnar1*$^{-/-}$ n = 4). Two-tailed one-way ANOVA test for difference of means ± s.d., followed by unpaired two-tailed t-tests of means of groups indicated by P-values. P-values < 0.05 were considered statistically significant. For gel source data, see Supplementary Fig. 1.

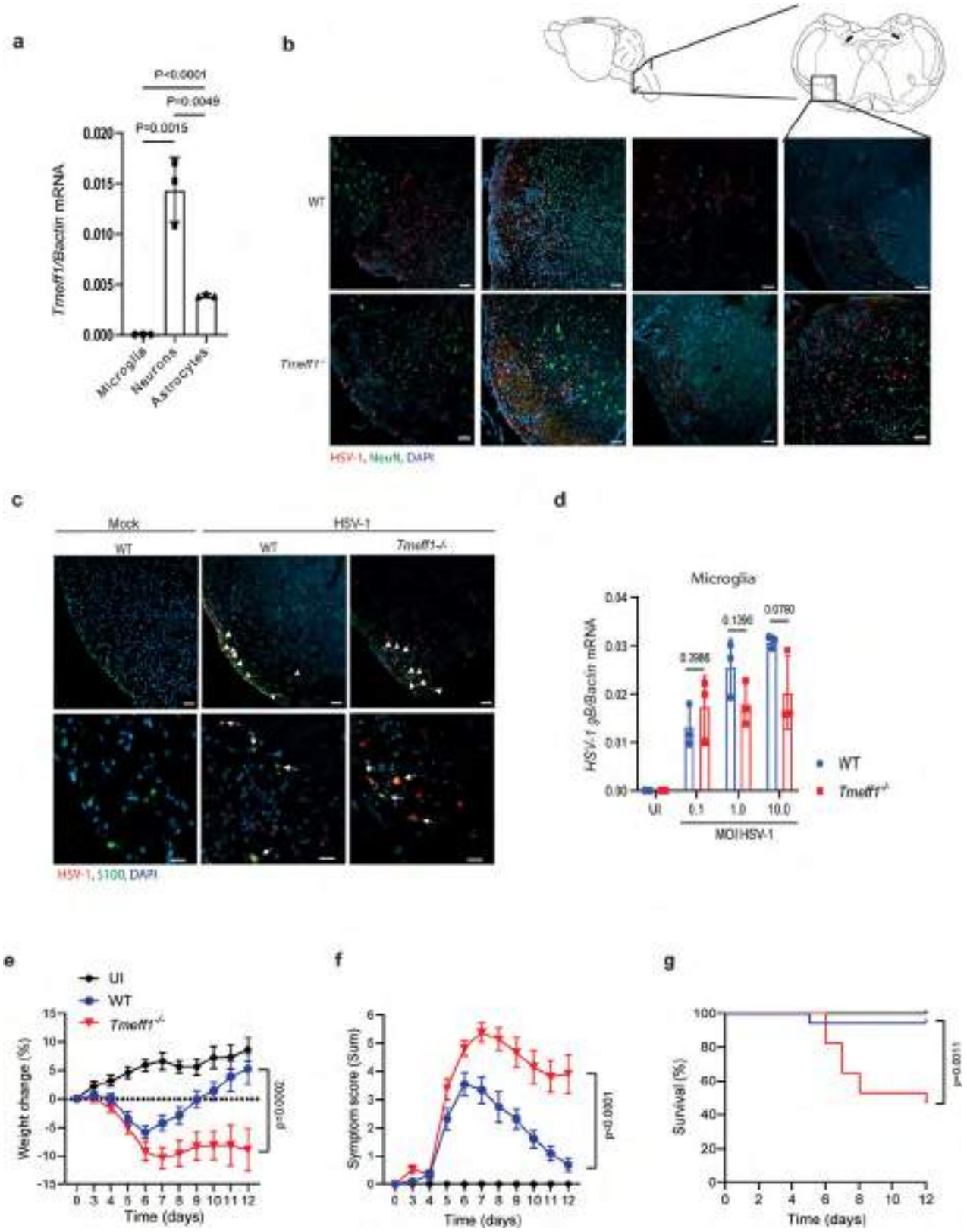

Extended Data Fig. 5 | See next page for caption.

Extended Data Fig. 5 | Immunohistochemical staining of HSV-1-infected brainstems. a, Total RNA was isolated from microglia, neurons, and astrocytes obtained from newborn C57BL/6N mice, and analyzed for *Tmeff1* mRNA levels relative to *Bactin* by RT-qPCR. Each dot represents one animal (n = 3). Two-tailed one-way ANOVA test for difference of means, followed by unpaired two-tailed t-tests of means of groups indicated by P-values. Error bars, ± s.d. P-values < 0.05 were considered statistically significant. **b-c**, Select examples of stainings visualized by fluorescence microscopy of brainstem sections from HSV-1-infected WT and *Tmeff1*$^{-/-}$ littermates (5 days p.i.) stained with DAPI, HSV-1 and, NeuN (neuron-marker) or DAPI, HSV-1, and S100 (astrocyte marker). Scale bar 10×, 50 µm; Scale bar 40×, 20 µm. Each brainstem (WT, n = 4 mice; *Tmeff1*$^{-/-}$, n = 5 mice.) is represented by images of 3 different anatomic bregma (−5.80, −6.72, −7.20 mm) and images of left and right side HSV-1+ foci, pr. bregma site. **d**, Primary mouse microglia infected with HSV-1 (McKrea) at increasing MOI. Viral *HSV-1gB* mRNA transcripts were evaluated by RT-qPCR and shown relative to *Bactin*, 24 h post infection. Each dot represents biologically independent samples (n = 3 pr genotype at different MOIs). **e-g**, *Tmeff1*$^{-/-}$ mice fully backcrossed for 10 generations to C57BL/6N background were infected in the cornea with HSV-1 (2×10^6 pfu/eye) and followed over time until reaching humane endpoint or recovering 100% of starting weight. **e**, % Weight change and **f**, Symptom scores. **g**, Survival curve (Uninfected, UI, n = 7; WT, n = 19, *Tmeff1*$^{-/-}$, n = 17). Dead animals were censored in the graphs, and thus represented in the graphs with the weight and symptom score at the time of death. Survival was analyzed using a Log-Rank Mantel-Cox test, and a comparison of disease development (e + f, weight change and symptom score) between the groups were compared with a Mixed-Effect Analysis with Geisser-Greenhouse Correction for comparison of multiple interacting variables (time and genotype). Error bars; S.E.M., P-values < 0.05 were considered significant.

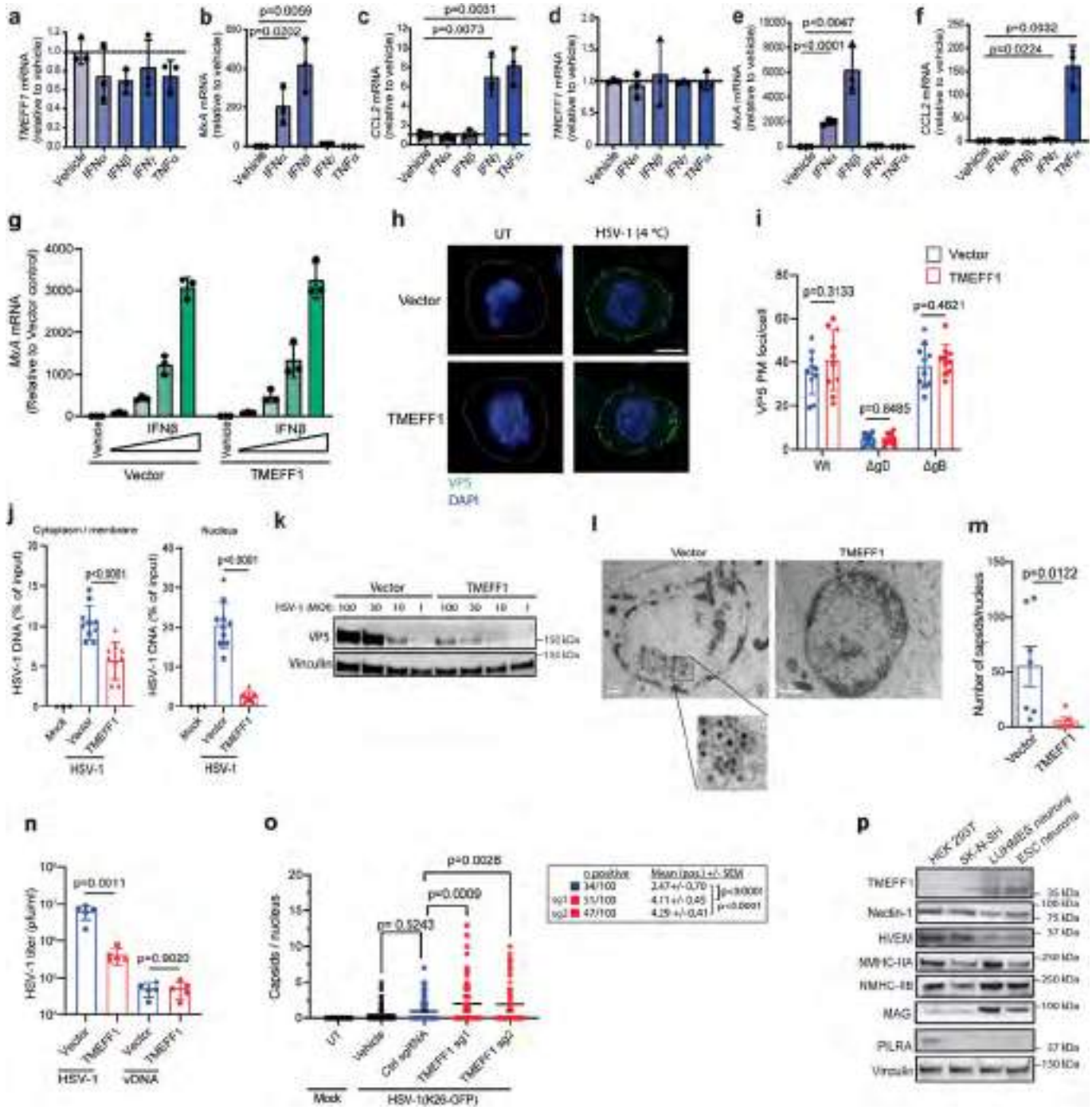

Extended Data Fig. 6 | See next page for caption.

Extended Data Fig. 6 | Characterization of TMEFF1 expression and function. Expression of *TMEFF1*, *MXA*, and *CCL2* in hESC-derived cortical neurons (**a-c**, n = 3 biological replicates) and SK-N-SH cells (**d-f**, n = 3 biological replicates) stimulated with IFNα (50 U/mL), IFNβ (100 U/mL), IFNγ (100 U/mL), or TNFα (50 ng/mL). for 6 h. Total RNA was isolated and examined for levels of mRNA transcripts by RT-qPCR. **g**, HEK293T cells were transfected with TMEFF1 or empty vector and stimulated with IFNβ at increasing concentrations (1, 3, 10, 30 U/mL). Total RNA was isolated 6 h later and examined for levels of mRNA transcripts for *MXA* (n = 3 biological replicates). **h**, HEK293T cells transfected with TMEFF1 or empty vector were treated with HSV-1 (MOI 100) at 4 °C, and stained for VP5 (HSV-1), and DAPI. Representative images are shown, scale bar = 10 um. **i**, HEK293T cells transfected with TMEFF1 or empty vector were treated with HSV-1 WT, Δ*gD*, and Δ*gB* (MOI 100) at 4 °C as illustrated in panel h. Following adsorption, cells were washed 3 time with ice-cold PBS. Cell-associated HSV-1 was quantified, and presented with each dot representing one cell (n = 10). **j**, DNA from cytoplasm/membrane or nuclear fractions of HEK293T cells transfected as indicated and infected with HSV-1 (MOI 1, 6 h). qPCR. data are presented as % viral DNA relative to infection doses (n = 10 biological replicates pr group, 4 individual experiments). **k**, HEK293T cells transfected with TMEFF1 or empty vector were infected with HSV-1 (MOI 1, 10, 30, 100) for 4 h. The cells were washed extensively, and cytoplasmic lysates were isolated and immunoblotted for VP5 and Vinculin (n = 4). **l**, HEK293T cells transfected with empty or TMEFF1 vector before infection with HSV-1 (MOI 15) for 12 h. The cells were fixed and visualized using electron microscopy. Scale bar, 1 µm. **m**, Quantification of virus capsids from the EM data, represented in panel k. Each data point represents one cell (n = 7). **n**, HEK293T cells were transfected with TMEFF1 or empty vector. Twenty four hours later, the cells were infected with HSV-1 (MOI 1) or transfected with HSV-1 DNA (500 ng/10^6 cells). Culture supernatants were isolated 24 h later, and viral yield was quantified by plaque assay (n = 5 biological replicates). **o**, LUHMES-derived WT and TMEFF1-deficient neurons were infected with HSV-1-K26GFP (MOI 50) in the presence of acyclovir. Cells were fixed after 2 h and subjected to confocal microscopy. GFP^+ spots were quantified in a blinded fashion. Data are presented as capsids per nuclei (DAPI, n = 100 nuclei). P value shown in graph is for comparisons between TMEFF1 and Ctrl. **p**, HEK293T cells, SK-N-SH, LUHMES-derived neurons, and ESC-derived neurons were lysed and subjected to immunoblotting for TMEFF1 and the indicated cellular proteins involved in HSV-1 entry. Vinculin was included as a control (n = 2). Data are shown as means of biological sample replicates ± s.d. Statistical analysis was performed using a two-tailed one-way ANOVA test followed by unpaired two-tailed t-tests of means indicated by P-values (a-f, i-j, m-o). $P < 0.05$ was considered statistically significant. For gel source data, see Supplementary Fig. 1.

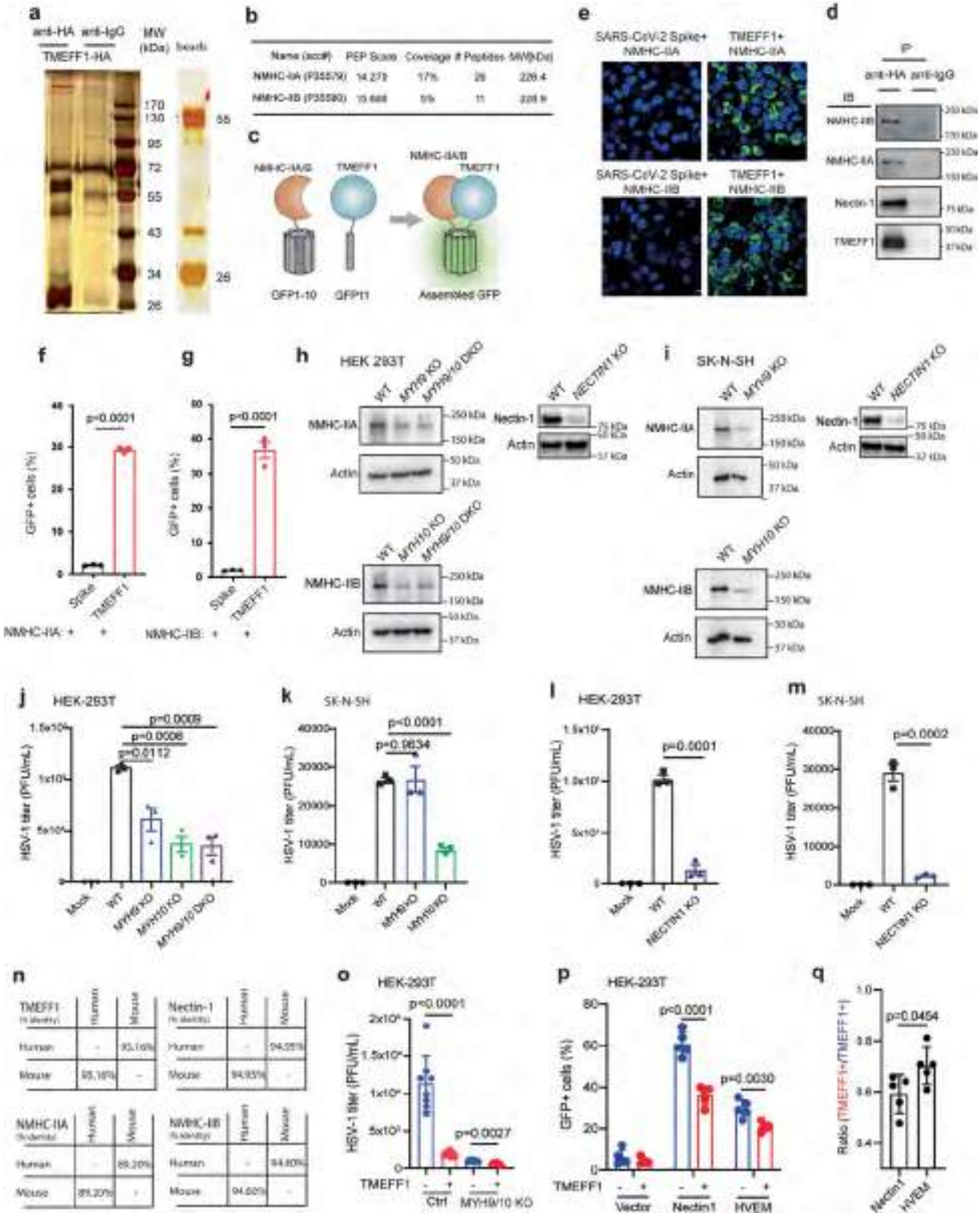

Extended Data Fig. 7 | See next page for caption.

Extended Data Fig. 7 | Identification and characterization of TMEFF1-interacting proteins. a, Lysates from HEK293T cells transfected with TMEFF1-HA were subjected to immunoprecipitation with anti-HA and anti-IgG beads, and visualized by silver staining of the SDS-PAGE gel (representative of n = 2 individual experiments). A > 170 kDa band highly abundant in the anti-HA precipitate (red box) was excised for mass spectrometry analysis. **b**, Data from the mass spectrometry-based identification of NMHC-IIA/IIB in the anti-HA-immunoprecipitate from TMEFF1-HA-transfected cells. **c**, Illustration of the principle behind split-GFP, allowing identification of in situ proximity of two fusion-proteins. **d**, Images of GFP signals in HEK293T cells expressing GFP1-10-fused NMHC-IIA (upper row), and NMHC-IIB (lower low) in combination with GFP11-fused TMEFF1 and SARS-CoV-2 spike as control. Scale bar, 20 µm (n = 3). **e**, Lysates from HEK293T cells transfected with TMEFF1-HA were subjected to immunoprecipitation with anti-HA and anti-IgG beads, and immunoblotted for NMHC-IIB, NMHC-IIA, Nectin-1, and TMEFF1. **f-g**, Quantification of the split-GFP signals by flow cytometry. Representation of the colocalization of NMHC-IIA-GFP1-10 or NMHC-IIB-GFP1-10 with TMEFF1-GFP11 and SARS-CoV-2 Spike GFP11, respectively. The data are shown as percentage of GFP-positive cells in individual biological samples (n = 3). **h-i**, Immunoblots for NMHC-IIA, NMHC-IIB, Nectin-1, and Actin in lysates from parental HEK293T or SK-N-SH cells or pools of cells treated for 48 h with gRNAs/Cas9 complexes targeting *MYH9, MYH10* and *NECTIN1* as indicated (n = 3). **j-m**, Parental HEK293T cells or pools of SK-N-SH cells treated with gRNAs/Cas9 complexes targeting *MYH9*, *MYH10*, *MYH9/10* DKO or *NECTIN1* were infected with HSV-1 (MOI 0.5). DKO; Double Knock Out. Supernatants were isolated 20 h later and viral yield was determined by plaque assay (n = 3 biological replicates). **n**, Percentage identity of the amino acid sequences between human and mouse TMEFF1, Nectin-1, NMHC-IIA, and NMHC-IIB. Alignment was performed using Uniprot. **o**, Parental HEK293T cells or pools of cells treated with gRNAs/Cas9 complexes targeting *MYH9* and *MYH10* were transfected with TMEFF1 and infected with HSV-1(MOI 0.5). Supernatants were isolated 20 h later and viral yield was determined by plaque assay (n = 8 biological replicates). **p**, *NECTIN1* deficient HEK293T cells were transfected with Nectin-1 (Nec1), HVEM and TMEFF1 as indicated and infected with HSV-1-GFP (MOI 0.5). The percentage of GFP^+ cells was analyzed 12 h post infection by flow cytometry (n = 5 biological replicates). **q**, The GFP ratio between the TMEFF1+ and TMEFF1÷ cells within the groups expressing Nectin-1 and HVEM was calculated (for each, n = 5 biological replicates). Data are ratios for individual data points normalized to means from the relevant TMEFF1÷ group. Statistical analysis was performed using an unpaired two-tailed t-test (f, g, q) and two-tailed one-way ANOVA test for difference of means (j-m, o, p), followed by unpaired two-tailed t-tests of means ± s.d. indicated by P-values (h-j). $P < 0.05$ was considered statistically significant. For gel source data, see Supplementary Fig. 1.

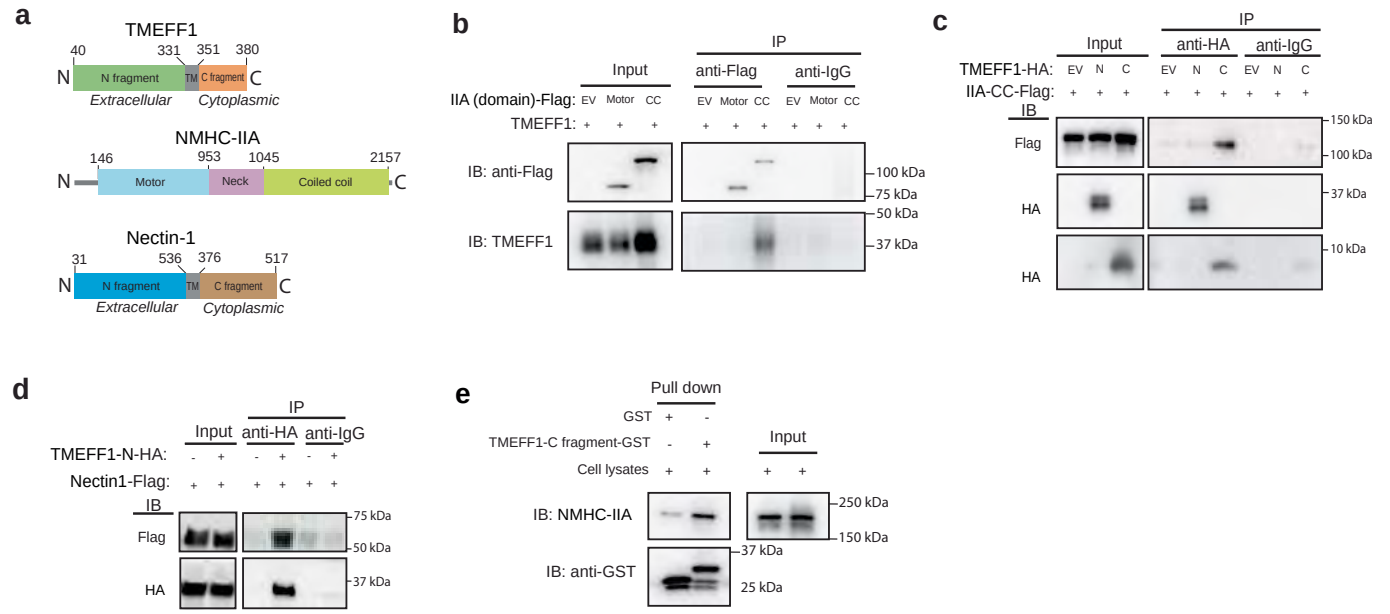

Extended Data Fig. 8 | TMEFF1 associates with NMHC-IIA and Nectin-1. **a**, Illustration of the domain organization of TMEFF1 and NMHC-IIA, and Nectin-1. **b**, HEK293T cells were transfected with TMEFF1 and the indicated NMHC-IIA domains (Flag-tagged). Lysates were subjected to IP with anti-Flag, and immuno-blotted for TMEFF1 and Flag. EV, empty vector; CC, coiled coil. Data isrepresentative of 3 independent experiments. **c**, The cytoplasmic C-terminal domain of TMEFF1 (TMEFF1-C) was expressed in bacteria fused to Glutathione-S-transferase (GST). GST pull-down was mixed with cell lysates from HEK293T cells, washed, and immunoblotted for NMHC-IIA and GST. Data representative of 2 independent experiments. **d**, Lysates from HEK293T cells transfected with Flag-tagged NMHC-IIA Coiled coil (CC) domain (IIA-CC-Flag) and HA-tagged N and C terminal fragments of TMEFF1 were subjected to IP with anti-HA, and immunoblotted as indicated. EV, empty vector. **e**, Lysates from HEK293T cells transfected with Flag-tagged Nectin-1 and HA-tagged N terminal fragment of TMEFF1 were subjected to IP with anti-HA, and immunoblotted as indicated.

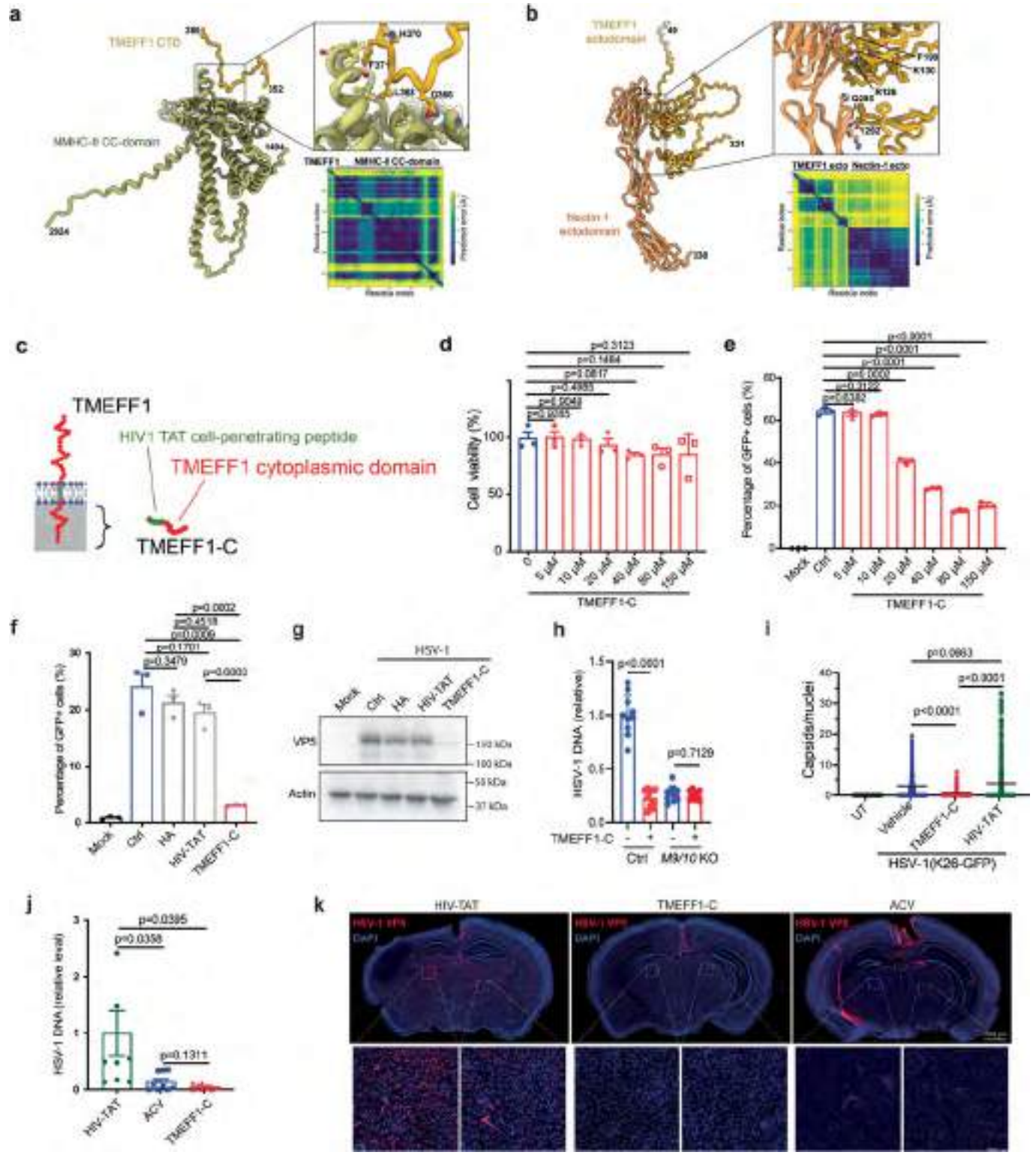

Extended Data Fig. 9 | See next page for caption.

Extended Data Fig. 9 | TMEFF1 interacts with NMHC-IIA and Nectin-1 to exert antiviral activity. a, Model from AlphaFold prediction of TMEFF1 C-terminal domain (gold) with NMHC-II coiled-coil domain (olive green). Window: enlarged view showing the TMEFF1 residues in closest proximity to NMHC-II residues to interact. The four TMEFF1 residues labeled were selected as candidates for mutational studies. Insert lower right, plot of model predicted aligned error scores. **b**, Model from AlphaFold prediction of TMEFF1 ectodomain (gold) with Nectin-1 ectodomain (orange). Window: enlarged view showing the TMEFF1 residues in closest proximity to NMHC-II residues to interact. The five TMEFF1 residues labeled were selected as candidates for mutational studies. Insert lower right, plot of model predicted aligned error scores. **c**, Illustration of the TMEFF1-C peptide consisting of the HIV1 TAT cell-penetrating peptide fused to the peptide corresponding to the cytoplasmic domain of TMEFF1. **d**, Viability of HEK293T cells after treatment with increasing amounts of TMEFF1-C peptide measured by LDH assay (n = 3 biological replicates). **e-f** Percentage of GFP+ cells post HSV-1 infection following treatment with TMEFF1-C and different control peptides. HEK293T cells were pretreated with peptides 6 h prior to infection with HSV-1-GFP (MOI 1). Cells were analyzed for GFP 17 h post infection by flow cytometry. Ctrl, control peptide; HA, influenza hemagglutinin (n = 3 biological replicates). **g**, Cells were treated as in panel f, and evaluated for HSV-1 replication by immunoblotting for HSV-1 VP5 in lysates isolated 17 h post infection. Data representative of 2 independent experiments. **h**, Parental HEK293T cells or pools of cells treated with gRNAs/Cas9 complexes targeting *MYH9* and *MYH10* were treated with TMEFF1-C peptide (40 μM) and infected with HSV-1(MOI 0.5). Nuclear DNA was isolated 3 h post infection, and HSV-1 DNA was measured by PCR (n = 10 biological replicates). **i**, LUHMES-derived neurons were treated with TMEFF1-C or HIV-Tat peptide (40 μM) and infected with HSV-1-K26GFP (MOI 50) in the presence of acyclovir. Cells were fixed after 2 h and subjected to confocal microscopy. GFP^+ spots were quantified in a blinded fashion (300 cells per group). Data are presented as capsids per nuclei (DAPI). **j**, C57BL/6 mice were treated with TMEFF1-C or control peptide (8 μL, 80 μM) or acyclovir (8 μL, 40 μM) and infected in the cornea with HSV-1 (2.6×10^6 PFU/eye). HSV-1 DNA levels in eye homogenates was determined on material isolated 2 days post infection (HIV-TAT and TMEFF1-C n = 8; ACV n = 10). **k**, Mouse brains were imaged by confocal microscope six days post infection. HSV-1 VP5 is shown in red and cell nuclei in blue. Scale bar: 1 mm (upper), 100 μm (lower). Data is represented as mean mean ± s.d. Statistical analysis was performed using two-tailed one-way ANOVA test followed by unpaired t-tests of means indicated by P-values (d-f, h-j). $P < 0.05$ was considered statistically significant. For gel source data, see Supplementary Fig. 1.

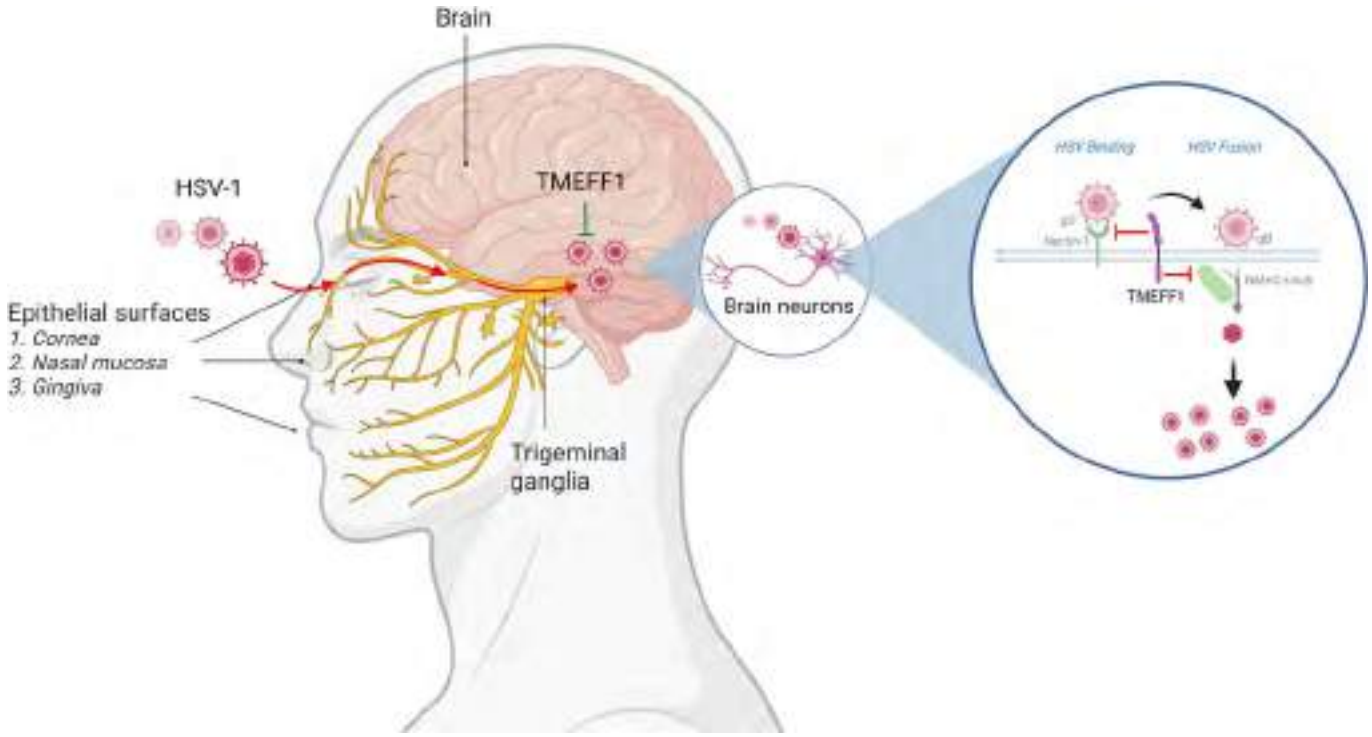

Extended Data Fig. 10 | Model for restriction of HSV-1 replication in CNS neurons by TMEFF1. Following HSV-1 infection at mucosal surfaces, the virus transports to the trigeminal ganglia for establishment of latency. In rare cases, the virus enters into the CNS where it can cause encephalitis. TMEFF1 is expressed preferentially in CNS neurons, and restricts HSV-1 replication by inhibiting viral entry. This involves interaction with the virus entry receptor Nectin-1 and the entry mediators NMHC-IIA/B. Created with BioRender.com.